MEASUREMENT OF MUSCULOSKELETAL MOTION USING VECTOR TISSUE DOPPLER IMAGING
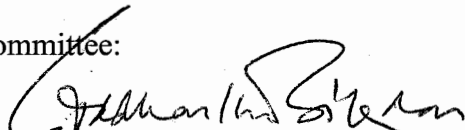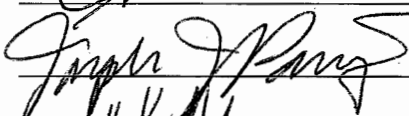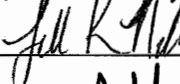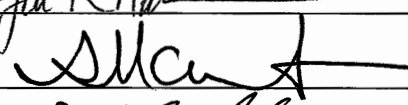
by

Avinash Eranki
A Thesis
Submitted to the
Graduate Faculty
of
George Mason University
In Partial fulfillment of
The Requirements for the Degree
of
Master of Science
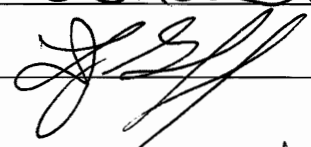Electrical Engineering

Committee:

_____ Dr. Siddhartha Sikdar, Thesis Director

_____ Dr. Joseph J. Pancrazio, Committee Member

_____ Dr. Jill K. Nelson, Committee Member

_____ Dr. Andre Manitius, Department Chair

_____ Dr. Lloyd J. Griffiths, Dean, The Volgenau
School of Information Technology and
Engineering

Date:____10/21/10____ Fall Semester 2010
George Mason University
Fairfax, VA

Measurement of Musculoskeletal Motion Using Vector Tissue Doppler Imaging

A thesis submitted in partial fulfillment of the requirements for the degree of Master of Science at George Mason University

By

Avinash Eranki
Bachelor of Engineering
Visveswariah Technological University, 2007

Director: Dr. Siddhartha Sikdar, Assistant Professor
Department of Electrical and Computer Engineering

Fall Semester 2010
George Mason University
Fairfax, VA

DEDICATION

This is dedicated to my father, Dr.E.V.S Prakasa Rao for being my best friend, my mentor, my coach (both basketball and swimming) and most of all, for being the extremely patient during my years of both poor performance and several injuries. His tremendous love, care and timely decisions during my near death injury will always be close to my heart.

This is also dedicated to my mother, E.N. Janaki, for her immense love and care that has helped me keep up my focus and goals till date. I will always be grateful to the support and enthusiasm she has given me during my years of low self-confidence.

Any amount of appreciation to my parents will be infinitesimally small, but I would still thank them for helping me to pursue my Masters and to be a better person.

ACKNOWLEDGEMENTS

TABLE OF CONTENTS

LIST OF TABLES

LIST OF FIGURES

ABSTRACT

MEASUREMENT OF MUSCULOSKELETAL MOTION USING VECTOR TISSUE DOPPLER IMAGING

Avinash Eranki, Master of Science

George Mason University, 2010

Thesis Director: Dr.Siddhartha Sikdar

The goal of this project is to develop, characterize and validate vector tissue Doppler imaging (vTDI) to measure dynamic musculoskeletal motion. We have developed a vector tissue Doppler imaging system using a clinical ultrasound scanner with a research interface. This system estimates motion in two or more independent directions using multiple electronically-controlled transmitters and receivers oriented in different directions. The vector tissue Doppler method combines the multiple velocity estimates producing a single velocity vector with magnitude and direction. We characterized this system *in vitro* by changing four parameters, namely, beam steering angle, depth of transmit focus, angle of velocity vector and

the depth of the scatterer relative to the beam overlap region. Our results show that changing these parameters have minimal effect on the velocity and angle estimates, and robust velocity vector estimates can be obtained under a variety of conditions. The mean velocity error was less than 6% of the maximum detectable velocity. We then performed some preliminary *in vivo* experiments to measure the velocity of the *rectus femoris* muscle group during a tendon tap in normal volunteers. Our goal was to investigate whether the muscle elongation velocities during a brisk tendon tap fall within the normal range of velocities that are expected due to rapid stretch of limb segments. We found that the equivalent velocities elicited during standard patellar tendon jerk test are within the range of velocities (3.26 rad s^{-1} to 8.23 rad s^{-1}) encountered in typical everyday activities, but the angular accelerations substantially exceeded the accelerations encountered in everyday activities (191.8 rad s^{-2} to 4038.6 rad s^{-2}). Our study provides the experimental evidence to support the non- physiological character of the tendon taps which is used during standard neurological tests.

We also investigated the feasibility of using vector tissue Doppler velocity estimates as a reliable clinical outcome measure in children with cerebral palsy (CP) and who have foot drop, or inadequate ankle dorsiflexion during

the swing phase of gait. We measured the *tibialis anterior* tendon contraction velocities during ankle dorsiflexion. Our preliminary results from this study show that tendon velocities estimated using vTDI have a strong linear correlation with the joint angular velocity estimated using a conventional 3D motion capture system. We observed a peak tendon velocity of 5.42 ± 1.01 cm/s during dorsiflexion and a peak velocity of 8.02 ± 2.33 cm/s during the passive relaxation phase of movement. Our preliminary studies demonstrate that vector Doppler may be used as clinical outcome measures and for studying efficiency of movement control. In the future, vector tissue Doppler imaging (vTDI) may be used to better understand gait disorders in patients suffering from cerebral palsy, spinal cord and brain trauma and other neuromuscular disorders.

CHAPTER 1: Introduction

Over the last four decades, ultrasound imaging has become the diagnostic method of choice for a variety of clinical conditions. This is because ultrasound imaging is a safe (non-ionizing radiation), portable and relatively lost cost diagnostic modality. These advantages have helped ultrasound imaging gain popularity in obstetrics & gynecology, echocardiography, vascular imaging and in general radiology.

One widely used mode of ultrasound in clinic is Doppler ultrasound. Doppler ultrasound provides quantitative velocimetry for vascular abnormalities. Doppler ultrasound is widely used for vascular examinations, echocardiographs and body imaging applications. Doppler technology has become quite sophisticated since the 1960's when single-element continuous wave instruments were first developed. Conventional Doppler imaging displays a spectral waveform of flow velocities over time. Pulsed wave Doppler enabled range gating to provide depth resolution. Simultaneous pulsed wave Doppler and conventional anatomical B-mode imaging (duplex

Doppler) allowed operators to localize flow in selected vessels. Color flow imaging was developed to overlay estimated velocities on a B-mode image to visualize blood vessels. Color flow is used in triplex systems (simultaneous B-mode, color-flow & Doppler spectrums) and is available in premium systems. New applications of Doppler ultrasound include tissue Doppler and elastography that enable assessment of the dynamics of tissue motion.

Doppler techniques applied to quantitatively measure musculoskeletal tissue motion has not been explored. Some potential applications of tissue Doppler ultrasound are quantitatively measuring muscle and tendon motion, in patients with cerebral palsy (CP), neuro-muscular diseases, spinal cord trauma, brain trauma and other gait related disorders. Currently in the clinic, joint kinematics and electromyography are used to evaluate musculoskeletal function. A quantitative method for direct measurements of muscle and tendon kinematics may lead to a better understanding of underlying pathophysiology. Ultrasound is uniquely suited for this application because it provides portable and real-time imaging in the physician's office. In the literature, a few methods have been proposed for estimating muscle and tendon motion using ultrasound. Some researchers measured the onset of

muscle activity [1]. Other methods rely on identification of landmarks in B-mode image sequences. Methods based on speckle tracking [2], elastography [3] or color Doppler [4] have also been proposed. Most of these methods lack the quantitative velocimetry and high temporal resolution that conventional Doppler methods can provide. However, conventional pulsed wave Doppler cannot directly be used for this application. Musculoskeletal tissue motion is generally along the surface of the skin (perpendicular to the direction of the ultrasound beam) and the motion of the tendon or muscle is in three dimensions during motion. One dimensional Doppler ultrasound can be inaccurate in estimating the true velocity of skeletal muscles and tendons when the motion is perpendicular to the ultrasound beam or the Doppler angle changes with time. Some additional inaccurate velocity estimates can also be produced due to variation of the angle between the beam and the direction of motion of muscles and tendons during movement. One approach to overcome these difficulties is to use vector Doppler. Some researchers have used a reference US beam to overcome the angle ambiguity [5]. Others have investigated angle independent vector velocity approaches like directional beamforming, synthetic aperture flow imaging and transverse oscillation [6]. We used cross beam based vector Doppler in our study.

Vector Doppler ultrasound estimates skeletal tissue motion in two or more independent directions using multiple transmitters and receivers oriented in different directions. The vector Doppler method combines the multiple velocity estimates producing a single velocity vector with magnitude and direction [7, 8]. Thus, vector Doppler can be used to estimate muscle and tendon velocities even if the motion occurs parallel to the skin surface. Since this method relies on spectral Doppler, it provides accurate quantitative estimates of tissue velocity, has higher temporal resolution over the speckle tracking method and does not rely on the visualization and tracking of anatomical landmarks in B-mode images.

Several research groups have come up with custom built vector Doppler systems. However, these custom built system lack flexibility to use in a clinical setting. The goal of this project is to develop, characterize and validate vector Doppler imaging using a clinical ultrasound scanner to measure tissue motion. We have developed a vector Doppler system based on a clinical ultrasound scanner with a research interface. We characterized this system *in vitro* by changing four parameters, namely, beam steering angle, depth of transmit focus, angle of velocity vector and the depth of the scatterer relative to the beam overlap region. We then performed some

preliminary *in vivo* experiments to measure the velocity of the *rectus femoris* muscle group during a tendon tap in normal volunteers. We also investigated the feasibility of using vector Doppler velocity estimates as a reliable clinical outcome measure by measuring the *tibialis anterior* tendon contraction velocities during ankle dorsiflexion in children with CP who have foot drop, or inadequate ankle dorsiflexion during the swing phase of gait. The measurements were compared with conventional joint kinematics estimated using a Vicon 612 (Lake Forest, CA, USA) 3D motion capture system. We obtained repeatable velocity estimates within the same patient for data collected 4 weeks apart. These preliminary results demonstrate that vector Doppler may be used as clinical outcome measures and for studying efficiency of movement control. We would like to continue to use vector tissue Doppler imaging (vTDI) to better understand gait disorders in patients suffering from cerebral palsy, spinal cord and brain trauma and several neuromuscular disorders.

CHAPTER 2: Brief background, Principles, Signal Processing and Issues with 1 Dimensional Doppler Ultrasound

History

Shigeo Satomura was one of the first to apply ultrasound techniques to measure the heart and peripheral and eye blood vessel pulsations in 1955 [9]. The system Satomura developed was a continuous wave system that resolved the Doppler shift frequency, but lacked depth resolution [10]. In 1960's, Baker and his colleagues found a way to obtain better depth resolution by pulsing the transmit signal [11]. This method is still used in the modern Doppler ultrasound systems.

One of the first multi beam systems consisted of single element Doppler transducers, both acting as transmitter and receiver (transceiver), arranged at 90º angle to each other. This was built by Fahrbach in 1970[12]. Several researchers over the last three decades have tried different ways to build and use a multi-dimension Doppler or Vector Doppler. A review paper by Dunmire et al. [6] has a brief list of researchers who worked on developing

new vector Doppler methods. Before describing the principles of vector Doppler, it is useful to review some important principles of ultrasound are explained in the next few sections of this chapter.

Basic Principles of Ultrasound

Sound waves propagate as longitudinal waves and require a medium to propagate. They cannot propagate in vacuum. Speed of sound depends on the material properties, density and the bulk modulus of the material. Typically, the speed of sound in human blood is about 1540 m/s. An ultrasound beam undergoes several effects when it interacts with a medium. Some of these effects are reflection, absorption and scattering. Acoustic impedance plays an important role ultrasound beam reflection and transmission. Larger the difference in acoustic impedance between the two tissue types, stronger the reflection at the interface of the two tissues or materials.

Scattering strength depends on the size of the structure. Diaphragm, large vessels, bones, cysts have a strong scattering effect, while blood is a weak scatterer of sound.

Attenuation is the energy lost due to interaction of sound with tissue either due to reflection, scattering or absorption. Ultrasound attenuation depends

strongly on the frequency. As the frequency increases, the attenuation increases. Attenuation also increases substantially due to the presence of air. For example, in lungs the attenuation coefficient is about 40 dB/cm-MHz as compared to blood which has an attenuation coefficient of 0.18 dB/cm-MHz. There are several modes of ultrasound imaging, such as A − Mode, B − Mode (Brightness - Mode), M − Mode (Motion - Mode), continuous and pulsed wave Doppler. This thesis work focuses on Doppler ultrasound imaging using a linear array transducer. Basic structure and functioning of an ultrasound transducer is explained in the next section. Before explaining the principles of Doppler, it is useful to understand how ultrasound signals are produced.

Basic Structure of a Transducer

When an ultrasonic transducer element is excited by a voltage or current signal, it converts electrical energy into acoustic energy during transmission and vice-versa on receive. Piezoelectric ceramic elements are commonly used as transducer elements like lead zirconate titanate (PZT). Design of ultrasound transducers has been explained in scientific literature [13-15];

however, their design details are often not revealed as they are considered proprietary.

The basic transducer is coated with a thin metallic layer which acts as an electrode. Wire connections to these electrodes allow the excitation applied to the element and the echo signal to be passed on to the receiver amplifier. When a ceramic material is used, a single or a multilayered wave plate is used to attach to the front face of the transducer to reduce impedance mismatch. This in turn helps in maximum acoustic energy to be transferred across the interface. Damping material is bonded to the back surface to reduce vibrations of the active element after the excitation pulse has ceased. The piezoelectric element and its attachments are placed in a metal cylinder. This metal cylinder is grounded to avoid any interference with surrounding electromagnetic signals that can interfere with the echo signals. Finally, the whole assembly maybe inserted in a plastic case and sealed to avoid ultrasound gel or water to leak into the transducer.

The frequency response of the transducer is of prime interest. Wideband transducers have become more popular than narrow band transducers since the wideband transducers have better spatial resolution. Alternatively, wideband transducers can transmit at 5MHz and receive at 10MHz. This

technique is employed in harmonic imaging. The percentage bandwidth maybe defined as

$$\Delta B(\%) = \frac{f_2 - f_1}{f_c} \times 100 \qquad (1)$$

Where f_1 and f_2 are lower and upper frequencies that fall by 3dB and f_o is the central frequency. The Q-factor is defines as:

$$Q = \frac{f_o}{f_1 - f_2} \qquad (2)$$

For PW Doppler, a Q of about 5 is preferred. Q of about 1- 3 is preferred for B – Mode imaging. This is to obtain good spatial resolution.

The ultrasound beam from an unfocused single element transducer has two primary regions/ zones: a near field (Fresnel zone) and a far field (Fraunhofer zone) as seen in Fig1.

$$N = \frac{D^2 f}{4c} ; \qquad (3)$$

where N = near field to far field transition point; f = frequency of sound; c = velocity of sound and D = diameter of the transducer face. Equation 3 gives

the near field to far field transition point of the ultrasound beam. Pattern of the ultrasound beam depends on physical structure of an ultrasound transducer and focusing.

$$N = \frac{D^2}{4\lambda}$$
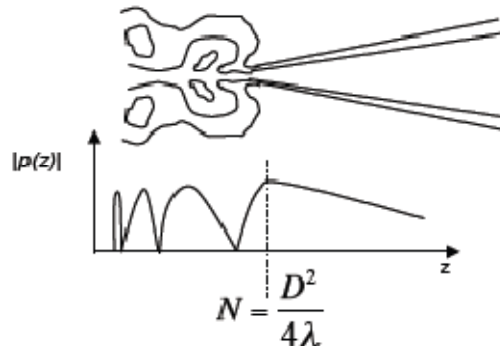
Figure1. Illustration of near field to far field transition. (Courtesy: Dr.S. Sikdar)

Array transducers consist of a separate elements placed in a linear or a curvilinear fashion. They have become popular and are now widely used is most ultrasound systems. Some of the several advantages of an array transducer over others are:

a.   Beam focusing can be electronically controlled.

b.   The ultrasound beam steering can be controlled electronically.

c.   They can be made small in size and they are compatible with current beamformers.

Steering and beam focusing are important in Doppler ultrasound applications. These are dependent on the structure of transducer. Some of

important principles of beam steering and focusing are explained in the next section.

Beam Focusing and Steering

The propagating ultrasound pressure wave may be focused or steered. Huygen's principle is one of the methods that can be used to understand focusing and steering. This principle articulates that each point of the wave front is responsible in producing a new set of wave fronts. These new or secondary waves are due to the summation of the all previously produced waves in the medium.

Huygen's principle was further expanded by stating that the amplitude of the wave at any given point equals the superposition of the amplitudes of all the secondary wavelets at that point. The Huygens- Fresnel Principle can be used to account for a broad range of phenomena. This principle helps understand focusing of an ultrasound beam in an array transducer. Ultrasound beams from array transducers are focused by transmitting from each element with a certain delay. This is illustrated in Fig.2, where the end transducer elements are fired first and the center transducer element is fired last.
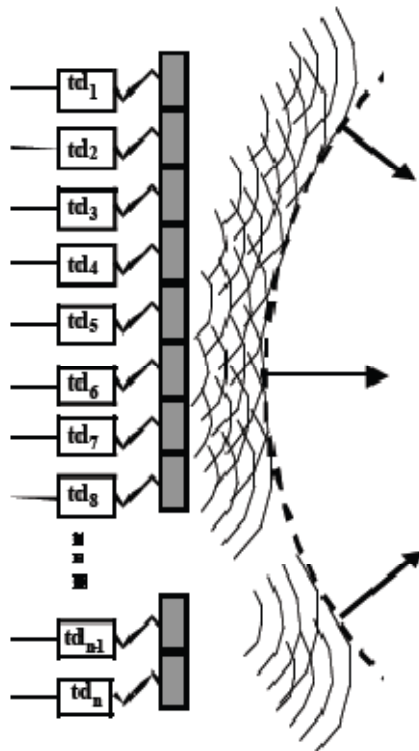
Figure2. Transducer elements are fired at a slightly different time to obtain focusing.
(Courtesy: Dr.S. Sikdar)
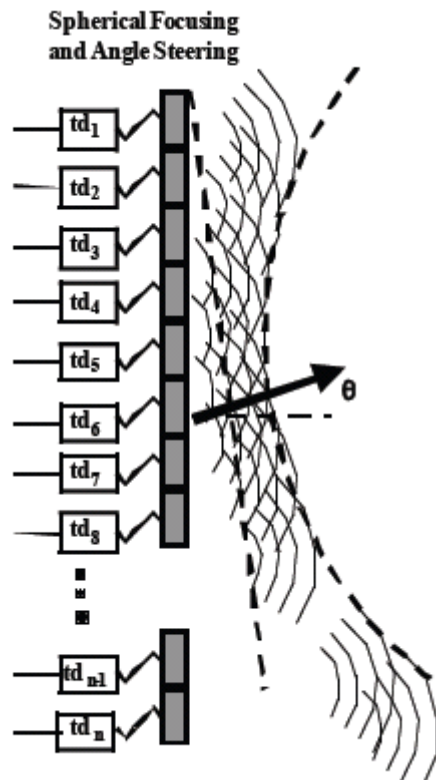
Figure3. Transducer elements are fired at a slightly different time to obtain focusing and steering. (Courtesy: Dr.S. Sikdar)

Steering the ultrasound beam is also possible by firing the transducer elements at different time intervals as seen in Fig.3.

Some of the other types of transducers available today are the single element, double element, linear array, curvilinear array, phased array, annular array, 3D/4D array, intravascular ultrasound (IVUS) and so on. Linear array transducer is widely used in Doppler examinations in clinic.

Some basic and important principles of conventional Doppler ultrasound are described in the next section.

Basic Principles of Doppler Ultrasound

The Doppler effect is the change in observed frequency of a wave due to motion of the scatterer. The observed frequency increases if the source or the scatterers are moving towards each other. The observed frequency decreases if the source or the scatterers are moving away from each other.

In medical ultrasonic applications, an ultrasonic beam is backscattered from blood or tissue. This relative increase or decrease in frequencies combines to give the resultant Doppler shift frequency. The Doppler shift frequency is given by:

$$f_d = \frac{2vf_t \cos\theta}{c} \qquad (4)$$

where v is the velocity of the scatterer relative to transmitter, f_t is the transmitted frequency, θ is the angle between the scatter and the axis of the transmit beam (isonation angle) and c is the speed of sound in that medium.

Doppler ultrasound has three modes; continuous wave (CW), pulsed wave (PW) and color Doppler.

CW systems are simpler of the three Doppler modes. In CW systems a continuous wave narrow band signal is used and the frequency of the received signal is modulated by the scatterer motion.
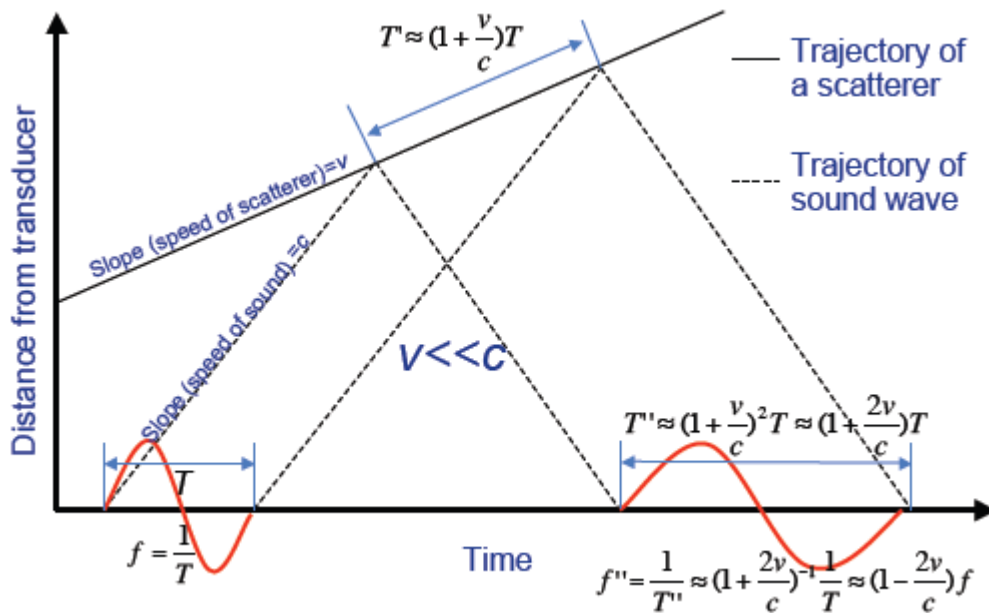
Figure4. Illustration the continuous wave (CW) Doppler effect. A pulse with a certain frequency '*f*'is transmitted. The frequency of the received signal, '*f*'' ' is modulated by the scatterer motion. The frequency of the received signal increases if the speed of the scatterer increases and vice-versa. (Courtesy: Dr.S. Sikdar)

Doppler frequency shift is given by,

$$ f_D = f'' - f = -\frac{2vf}{c} \tag{5} $$

16

The advantages of CW Doppler are:

a. Easy to use: few operator controls; simple point and shoot.

b. Inexpensive instrumentation.

The disadvantage of CW Doppler is that it lacks depth resolution since the transducer is continuously transmitting and receiving and hence it is not possible to know at what depth the scatterer is. Some of the applications of CW Doppler are fetal heart rate, cardiology and peripheral blood pressure with both ankle and arm at rest.

If we need to have depth resolution, then we need to transmit a finite duration pulse at regular intervals of time, as seen in Fig5. The time interval between transmitting and receiving a pulse can be used to calculate the location and the depth of the object. However, this cause's range ambiguity since the signals arriving at the transducer at a given time may be echoes from the latest transmission pulse, previous pulse or even earlier transmitted pulses.
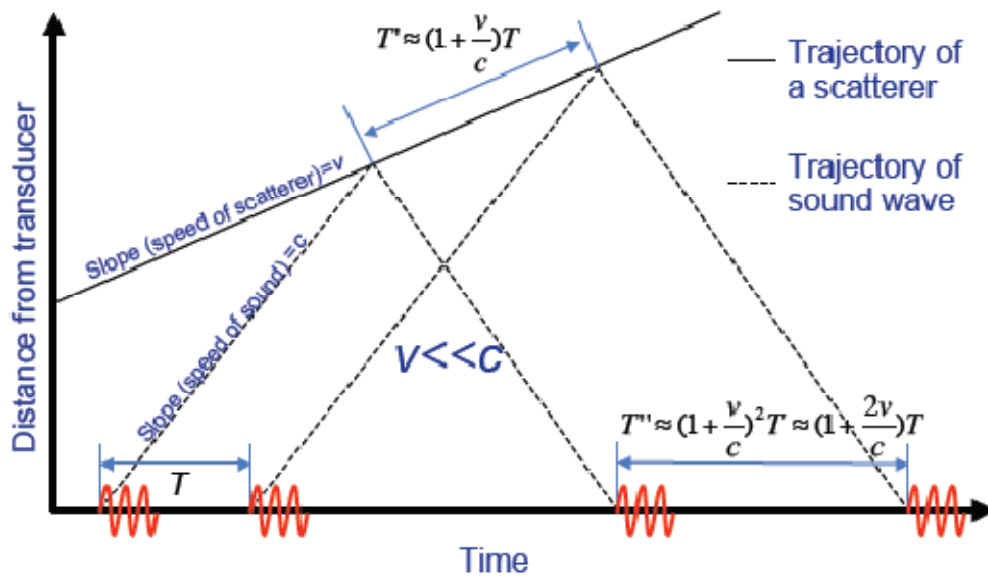
Figure5. Illustration of a PW Doppler system that overcomes the disadvantage of depth ambiguity in CW systems. Two pulses with a time gap of T are transmitted. Time delay between these two pulses (T') is modulated by scatterer motion. The time delay (T') increases with increase in scatterer motion and vice-versa. (Courtesy: Dr.S. Sikdar)

One approach to overcome this problem is by increasing the pulse repetition frequency (PRF) beyond the maximum required. Pulse repetition frequency (PRF) is the number of pulses transmitted by the system within a second. The upper PRF limit is given by the time interval required for the echoes to arrive from a sample volume at a certain depth. The maximum Doppler shift that can be unambiguously detected is:

$$f_d(\max) = f_s/2 \tag{6}$$

18

If the Doppler shift frequency exceeds $f_s/2$, aliasing occurs, causing the perceived frequencies to wrap around, eg., a high positive shift $> f_s/2$ would be interpreted as a high negative shift $> -f_s/2$. Doppler shift frequencies are normally interpreted between $-f_s/2$ *to* $f_s/2$. However, it can also be interpreted between any other range of frequencies, for example from $-f_s/4$ to $3f_s/4$.

Beamforming, demodulation, filtering and velocity estimation are some prime signal processing blocks required to process the raw Doppler data. Some basic concepts of signal processing in Doppler ultrasound are briefly explained in the next section.

Signal Processing

Beamformers

Some of the basic signal processing blocks in ultrasound are beamforming, demodulating, filtering and velocity and angle estimators.

In array transducers, timing of excitation of each element and the number of elements excited can all be controlled and altered rapidly, as seen in Fig.3. The shape of transmit beam changes based on delays applied at each

transducer element. The received signal at each element can be digitized accurately and rapidly to preserve amplitude and phase information. The Ultrasonix Sonix RP® and Sonix Touch® digitize data at 40MHz. The beamformer applies time delays to the shape of the ultrasound beam. It also performs:

- Apodisation on transmission – by weighting the size of exciting signals applied to each element to improve the beam shape and in particular reduce side lobes.

- Dynamic focusing on reception – by changing the delay pattern applied to echo signals from elements of an array, the array can be focused dynamically at the depth of the target which produced the echoes. This dynamic focusing is an attractive feature of array transducers.

- Apodisation on reception – by weighting the gain applied to each echo signal to improve the beam shape and also reducing side lobes.

- Variable aperture on transmission and reception – by varying the number of elements used for each focal range the sharpness of the focus can be improved.

Demodulation

Motion of scatterers modulates the phase of the received RF carrier signal.

Directional demodulation is an important component in Doppler ultrasound.

This is accomplished by using quadrature phase detection, by coherently

demodulating the received Doppler signal, both with the master oscillator

and with the signal derived from the master oscillator but shifted by 90º.

For the sake of simplicity, let us consider an ultrasound signal consisting of

three distinct components: the carrier, signal resulting from motion toward

the transducer and away from the transducer. Such a signal may be written

as:

$$S(t) = A_0\cos(\omega_0 t + \Phi_0) + A_f\cos(\omega_0 t + \omega_f t + \Phi_f) + A_r\cos(\omega_0 t - \omega_r t + \Phi_r) \quad (7)$$

where A, ω, Φ refer to amplitude, angular frequency and phase respectively.

The subscripts 0, f and r represent carrier, forward and reverse signals

respectively.

Multiplying Eq7 by $\cos(\omega_0 t)$, we get:

$$D(t) = \frac{1}{2}A_0[\cos(\Phi_0) + \cos(2\omega_0 t + \Phi_0)] +$$

$$\frac{1}{2}A_f[\cos(\omega_f t + \Phi_f) + \cos(2\omega_0 t + \omega_f t + \Phi_f)] +$$

$$\frac{1}{2}A_r[\cos(\omega_r t - \Phi_r) + \cos(2\omega_0 t - \omega_r t + \Phi_r)] \quad\quad\quad (8)$$

Filtering out the DC component and the high frequency components at $2\omega_0$, we get:

$$D'(t) = \frac{1}{2} A_f \cos(\omega_f t + \Phi_f) + \frac{1}{2} A_r \cos(\omega_r t - \Phi_r) \qquad (9)$$

Multiplying the signal given by Eq.7 by $\sin(\omega_0 t)$ leads in a similar way to a filtered quadrature signal, $Q'(t)$, given by:

$$Q'(t) = -\frac{1}{2} A_f \sin(\omega_f t + \Phi_f) + \frac{1}{2} A_r \sin(\omega_r t - \Phi_r) \qquad (10)$$

or

$$Q'(t) = -\frac{1}{2} A_f \cos(\omega_f t + \Phi_f + \pi/2) +$$

$$\frac{1}{2} A_r \cos(\omega_r t - \Phi_r - \pi/2) \qquad (11)$$

It can been seen from comparing Eq.9 with Eq.11 that for a signal resulting from flow which is solely towards the transducer the direct signal lags the quadrature signal by 90º, and if the flow in solely away from the transducer, the direct signal leads the quadrature signal by 90º. Further processing is required to obtain signals that are purely forward and reverse. Phasing filter method is one of the ways to separate the forward and reverse flow signals. A common practical and digital implementation of the phasing filter was suggested by [16]. This implementation is based on a wideband Hilbert

transform, which produces a 90º phase shift in the direct input. This is illustrated as follows:
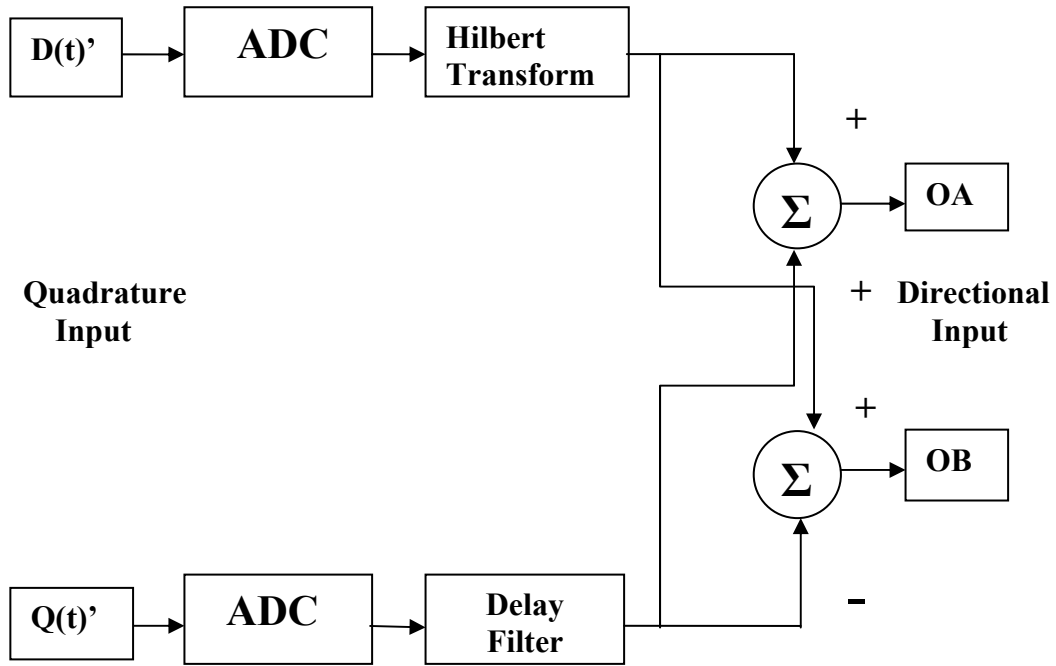
Figure.6 Phasing filter implementation described by Aydin and Evans to produce forward and reverse flow signals.

Both the direct and quadrature channels are phase-shifted by 90º and added to the other (unshifted) channel, and this results in two completely separate flow channels.

Phase shifting the direct signals given by Eq.(10) leads to:

$$D^{+}(t) = -\frac{1}{2} A_f \sin(\omega_f t + \Phi_f) - \frac{1}{2} A_r \sin(\omega_r t - \Phi_r) \qquad (12)$$

Adding this signal to the unshifted 'quadrature' signal Eq.12 eliminates the reverse flow and gives:

$$F(t) = -A_f \sin(\omega_f t + \Phi_f) \tag{13}$$

Similarly, shifting the quadrature signal by 90^0 gives:

$$Q^+(t) = -\frac{1}{2} A_f \cos(\omega_f t + \Phi_f) + \frac{1}{2} A_r \cos(\omega_r t - \Phi_r) \tag{14}$$

Which when added to the unshifted direct channel Eq.9 eliminates the forward component and yields:

$$R(t) = A_r \cos(\omega_r t - \Phi_r) \tag{15}$$

Clutter Filtering

Clutter filtering is an important step in processing Doppler signals. Clutter is relatively high amplitude and low frequency echoes from stationary or near-stationary targets. It originates from surrounding tissues and/or slow moving vessel walls. The clutter signals are typically below 1 KHz and are typically higher by 40 – 60 dB than the actual signal from blood [17] and must be removed if accurate estimation of blood flow or tissue motion has to be made. High pass filters are commonly used as clutter filters. We used a

fourth order Chebyshev high pass filter with variable cut-off frequencies for our experiments.

The received Doppler signal in time domain

In pulsed wave Doppler, a pulse is emitted at regular intervals of time. Each pulse emitted gives rise to a 'fast-time' (E_0, E_1, etc. in Fig.7 & 8). This is one line of RF data. Over a period of time several such fast-time signals are collected, which is termed as 'slow-time'. This is illustrated in Fig.7 & 8. Each pulse is transmitted at a calculated interval of time called pulse repetition interval (PRI). The pulse repetition frequency is given by PRF = $\dfrac{1}{PRI}$. If the scatterer is not moving, there is no change in each fast-time over slow-time. In other words the RF signals (fast time signals) along the slow time are exactly identical and one behind the other. If the scatterer is moving, then there is change in each fast-time over slow-time depending on the velocity and direction of the scatterer. Figure 7 & 8 illustrates this effect when the scatterer is stationary and scatterer is moving respectively.

Narrowband velocity estimation using the spectrogram

Fig.9 shows fast- time in one dimension and slow – time in another dimension of a raw RF data collecting *in vitro* using a calibrated string

phantom. The Fourier transform may be used to estimate the power spectrum by the periodogram approach. This is done by selecting a certain point in the fast-time and using a sliding window through slow-time, we obtain a trace whose Fourier transform is obtained to get the 1D frequency response. Velocity is then calculated using:

$$v_{max} = \frac{c \times PRF}{4 \times f_c} \qquad (16)$$
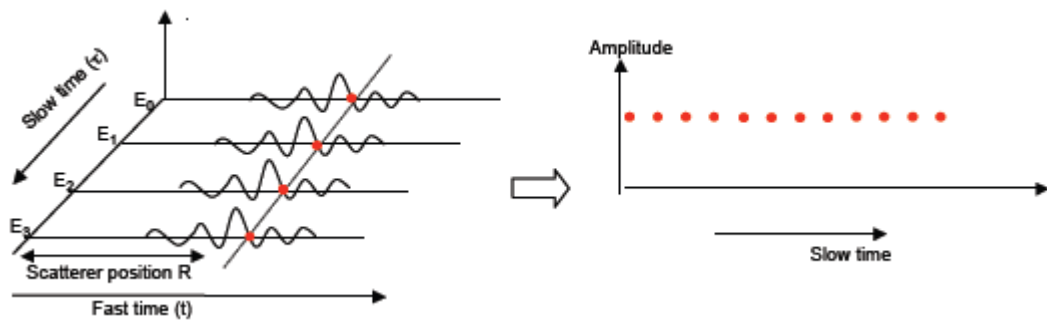
Figure7. Pulsed wave (PW) Doppler signal of a stationary scatterer. (Courtesy: Dr.S. Sikdar)
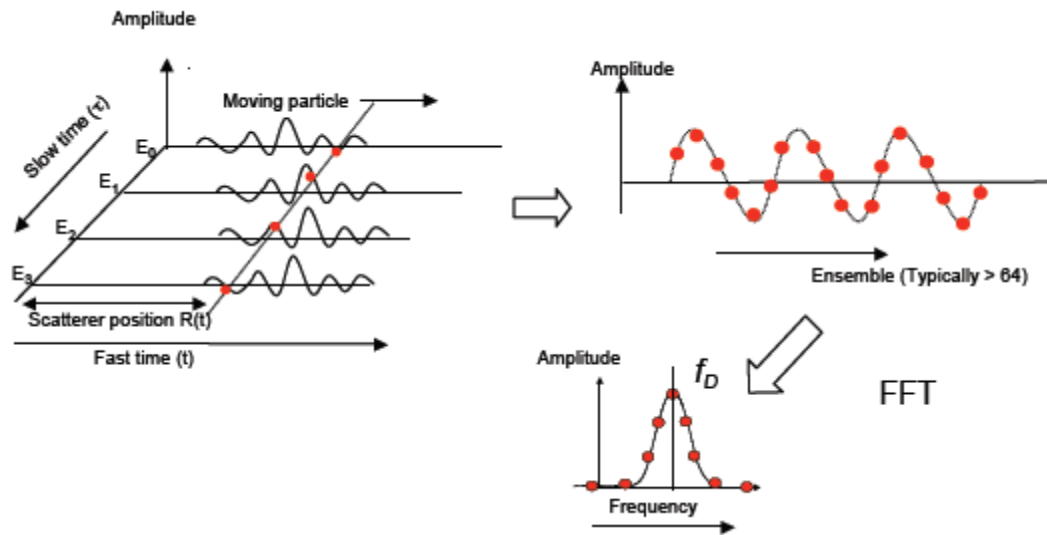
Figure8. Pulsed wave (PW) Doppler signal of a moving scatterer. (Courtesy: Dr.S. Sikdar)
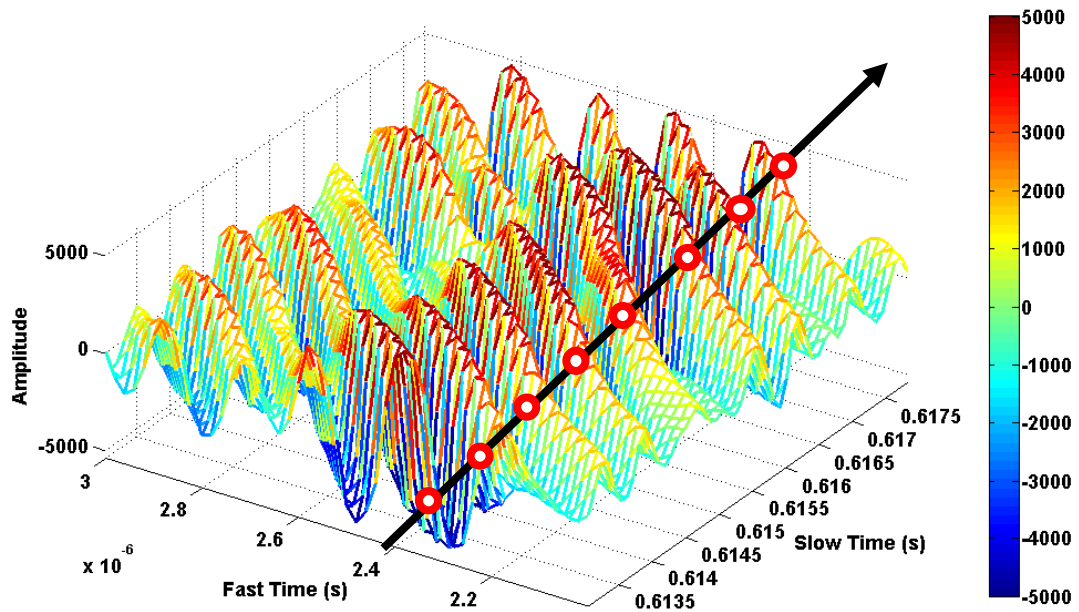
Figure9. An example of fast time and slow time of a Doppler M-Mode using a calibrated string phantom. Black line with red dots represents the line selected over slow-time to calculate the velocity of the scatterer.

However, this method of velocity estimation is a narrow band estimator and suffers from poor velocity estimation during high velocities of the scatterer. It is however possible to slightly reduce the variance of the estimate by averaging over a number of independent estimates known as Bartlett' procedure. The spectral variance is inversely proportional to the number of estimates that are averaged. The spectral resolution is determined by the length of the data sample obtained. For example, if we consider the entire data sample of length 'X', the variance would be $P(\omega)^2$ and the resolution is 1/X. If we split the data sample into 'N' segments, the variance would be $P(\omega)^2/N$ and the resolution would be X/N. An implicit assumption often made is that the data is stationary. However, this is not true in practice. It is the length of the signal assumed to be stationary that defines the length of the segment 'N' used to produce a spectral estimate of a Doppler signal. For example Doppler signals in arteries may vary for every 20-30 ms and hence it is not possible to obtain a frequency resolution better than 50-100 Hz. Another approach to average spectral estimates from overlapping segments as described by Welch in 1967[18]. This helps further reduce spectral variance. However, these estimation methods could still have high variance

due to the large non-stationary broadening during acceleration or deceleration phase. One approach to reduce such variance is to use a 2D FFT as described in the section below.

Autocorrelation method for estimating mean velocity

Once the Doppler signal is high pass filtered to remove the low frequency echoes due to stationary or slow moving objects, velocity estimation may be performed by calculating the mean frequency, bandwidth and power. One of the several methods to estimate velocity is autocorrelation, which is a mean velocity estimator. The formal way of deriving the autocorrelation estimator was given by Kasai *et al* (1985) [19].

The mean angular frequency, $\overline{\omega}$ of a Doppler power spectrum, $P(\omega)$, may be defines as:

$$\overline{\omega} = \frac{\int\limits_{-\infty}^{\infty} \omega P(\omega) d\omega}{\int\limits_{-\infty}^{\infty} P(\omega) d\omega} \qquad (17)$$

while the variance is defined as:

$$\sigma^2 = \frac{\int\limits_{-\infty}^{\infty}(\omega-\overline{\omega})^2 P(\omega)d\omega}{\int\limits_{-\infty}^{\infty}P(\omega)d\omega} \qquad (18)$$

$$\Rightarrow \sigma^2 = \overline{\omega}^2 - (\overline{\omega})^2$$

Further, the autocorrelation function $R(\tau)$ is related to $P(\omega)$ by the Weiner-Khinchin theorem :

$$R(\tau) = \int\limits_{-\infty}^{\infty}P(\omega)e^{j\omega\tau}d\omega \qquad (19)$$

Differentiating equation 19 with respect to τ, we get two further relationships:

$$\dot{R}(\tau) = j\int\limits_{-\infty}^{\infty}\omega P(\omega)e^{j\omega\tau}d\omega \qquad (20)$$

and

$$\ddot{R}(\tau) = -\int\limits_{-\infty}^{\infty}\omega^2 P(\omega)e^{j\omega\tau}d\omega \qquad (21)$$

Equations (20) and (21) may be written in terms of autocorrelation functions for zero lag to give:

30

$$\overline{\omega} = -j\frac{\dot{R}(0)}{R(0)} \qquad (22)$$

and, $\qquad \sigma^2 = \left(\frac{\dot{R}(0)}{R(0)}\right)^2 - \frac{\ddot{R}(0)}{R(0)} \qquad (23)$

Also the average power of the signal, $\overline{W}$, is given by the autocorrelation function at $\tau = 0$, that is:

$$\overline{W} = R(0) \qquad (24)$$

It is possible to evaluate equations (17) and (18) directly, but Kasai *et al.*(1985) pointed that if autocorrelation is treated as:

$$R(\tau) = |R(\tau)|e^{j\phi(\tau)} = A(\tau)e^{j\phi(\tau)} \qquad (25)$$

where A(τ) is a real function of τ, and $\phi(\tau)$ a real odd function of τ, then the following approximation is valid:

$$\overline{\omega} = \dot{\phi}(0) \approx \phi(T)/T$$

$$= \frac{1}{T}\arctan\frac{\mathrm{Im}\,R(T)}{\mathrm{Re}\,R(T)} \equiv \frac{1}{T}\arg R(T) \qquad (26)$$

and

$$\sigma^2 \approx \frac{2}{T^2}(1 - \frac{|R(T)|}{R(0)})$$

<div align="right">(27)</div>

where T is the time between subsequent ultrasonic pulses. The mean angular frequency and variance may be calculated from its autocorrelation magnitudes and phases at lags of $\tau = 0$ and $\tau = $ T. Autocorrelation is a narrow band estimator and tends to have higher variance in estimating velocity during sudden change in velocity and high velocities. Also, in 1D spectral estimation the full bandwidth of the spectrum is used. This is disadvantageous when the velocities are high or during acceleration/deceleration where the variance is high. A wide band estimator like 2D Fourier transform could better estimate velocities.

Broadband velocity estimation using 2D Fourier Transform
Traditionally the Doppler signal obtained from a single direction through the tissue is viewed as a one-dimensional signal containing a series of in-phase and quadrature phase samples which vary with time. In the case with pulsed wave Doppler techniques, however, either the RF signal or the demodulated components may be viewed as a two dimensional (2D) signal, where one

dimension corresponds to depth (fast - time) and the other dimension corresponds to frame number (slow - time), as shown in Fig.9.

The 2D Fourier transform is well known in image processing and other 2D signal processing applications. In practice, pulsed wave system transmit a range of frequencies producing constant velocity Doppler shifts which are mapped as a radial line passing through the origin with the slope proportional to the velocity of the scatterer. Spectral broadening associated with the width or the time duration of the transmitted pulse, which will lead to frequency spread in the Doppler frequency direction and thus in the RF direction too. The resultant effect is an elliptical shape in the 2D Fourier space as seen in Fig.10.
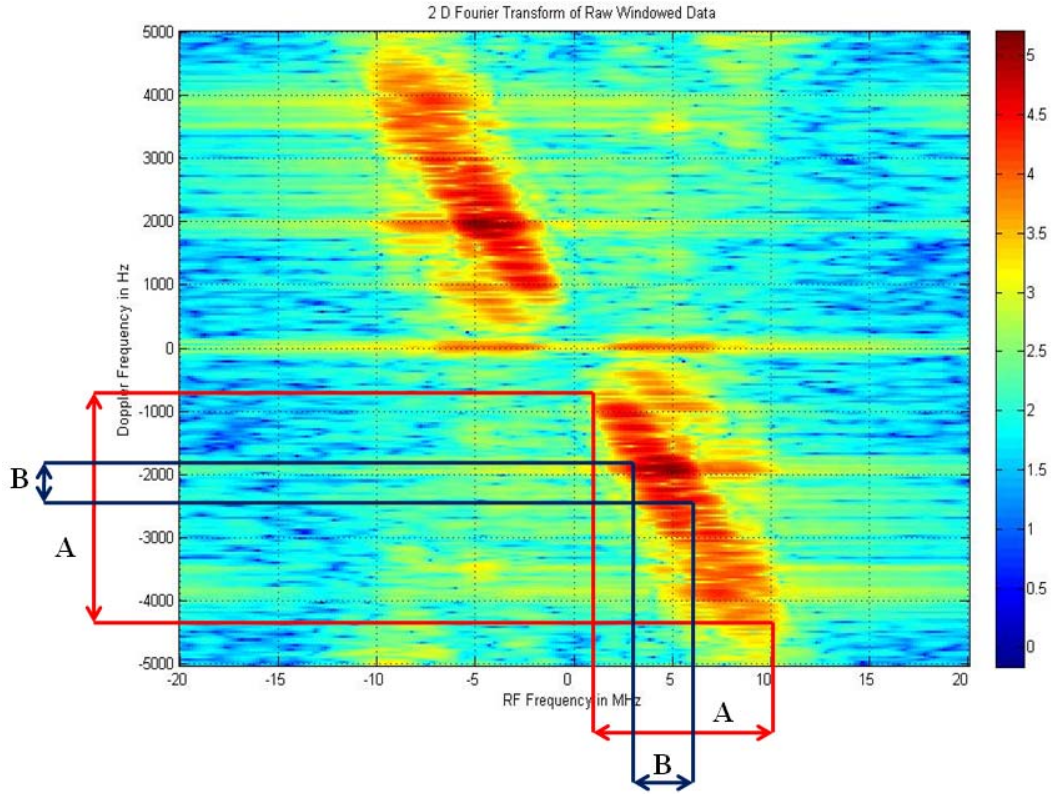
Figure10. A 2D Fourier transform of a demodulated RF data. The carrier frequency was set to 5MHz and the Doppler shift frequency was 2000Hz. A corresponds to a narrow band estimator (autocorrelation) and B corresponds to a wide band estimator (2D Fourier transform).

Loupas and Gill (1994) [20] showed that conventional narrow band processing is equivalent to evaluating the 2D Fourier transform along the line given by $f_{RF} = f_c$, where f_c is the center frequency of the transmitted ultrasound pulse. In general we could write this as:

$$P_{1D}(f_d) = P_{2D}(f_{RF} = f_c, f_d) \qquad (28)$$

A small bandwidth is selected, i.e, $f_c \pm$ BandWidth, and this is projected onto the Doppler frequency axis. This approach helps reduce variance due to sudden acceleration or deceleration of the scatterer and fares better than a narrow band estimator like autocorrelation. Even with a broadband estimator like 2D Fourier transform, there are some inherent issues with conventional Doppler ultrasound that make velocity estimation inaccurate. Some of these are explained in the next section.

Issues with 1D Doppler Ultrasound

Conventional duplex 1D-Doppler ultrasound has been well established for over 2 decades in detecting blood flow velocity. 1D Doppler spectrum estimates blood flow velocity along the direction of the ultrasound beam. The velocity magnitude estimated from the 1D Doppler assumes the flow vector to be parallel to vessel axis. In the case of an artery the flow vector is blood flow. The flow vector can also be motion of skeletal muscles or tendons. The resultant velocity magnitude is calculated from the beam to vessel axis angle measured using an angle cursor. In several cases, secondary flow phenomenon are introduced due bifurcations, curves and

also due to anatomical structures in the human body. Also, skeletal muscles and tendons tend to move along the surface of the skin. Assumptions made about the blood flow or tissue motion may not hold well in such scenarios. This can result is erroneous determination of true velocity of the flow vector and other derived parameters like stress, strain and strain rate. Interpretation of such results may lead to wrong clinical outcomes and conclusions.

Further complications can arise if the sonographer sets the angle cursor incorrectly or inconsistently. The beam to vessel axis angle of 60^0 is accepted by some laboratories and other laboratories accept lesser than 60^0 and sometimes smaller the better. In some cases, the beam to vessel axis angle may not be the same for consecutive studies on the same patient. Also, the anatomical landmark to which the angle cursor is aligned may vary.

Also, current clinical duplex Doppler does provide a spectrum of velocity components within a sample volume for over a period of a short duration of time (10-20ms). The spectral output does not reveal the differences in the flow direction due to turbulence or disturbed flow. In the case of muscle or tendon motion, 1D Doppler spectrum may not be able to provide the true

dynamics of motion. Investigating these more detailed aspects of blood flow and tissue motion may lead to additional and improved diagnostic criteria.

These issues with conventional 1D duplex Doppler have led to the development of angle independent Doppler systems. One such approach is vector Doppler. These systems reconstruct the true velocity of blood flow or tissue motion by combining multiple velocity vectors. However, vector Doppler systems have been in research for over two decades, but with little success in clinic due to the lack of commercial systems supporting vector Doppler.

Vector Doppler systems use conventional Doppler from two or more independent directions using multiple transmitters or receiver pairs. This may be accomplished using multiple transducers arranged in a variety of geometric positions. Several research groups have built vector Doppler using custom built systems [7, 8]
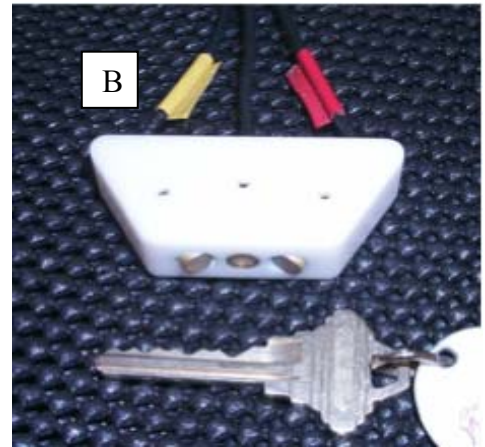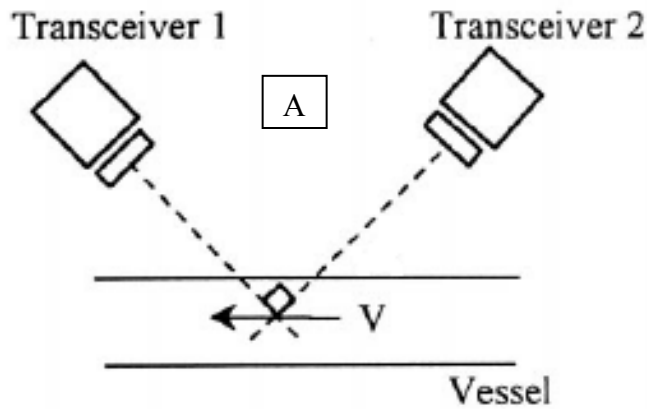
Figure11. Basic vector Doppler geometry with 2 transceivers shown in 'A'. A custom built vector Doppler system is also shown in B (Courtesy: Dr. Kirk Beach).

However, these custom built systems have limited flexibility as seen in Fig.11(B). The limited flexibility in a system shown in Fig. 11(B) is due to the inability to change the number of elements in the aperture and the beam steering. Another approach to vector Doppler is to use a clinical system with an array transducer and electronically split the array into multiple transmitters and receivers and steer these beams at different angles. Such systems have an advantage of electronically controlling transmitter and receiver beam geometries and perform experiments in a clinical setting with simultaneous imaging. However, vector Doppler systems have not been extensively investigated. We have developed a vector Doppler system based on a clinical ultrasound scanner with a research interface. We performed *in vitro* characterization of a vector Doppler system based on a clinical scanner. In particular, we investigated the robustness of the vector Doppler velocity

estimates to change in beam steering angle, depth of the velocity vector, angle of the velocity vector and transmit focus depth.

There are several applications of Doppler ultrasound and vector Doppler ultrasound. The focus of our research is to understand and come up with a diagnostic tool to quantitatively measure muscle and tendon motion in patients with cerebral palsy and foot drop. Eventually we would like to use this technique to understand the dynamics of musculoskeletal motion is patients with cerebral palsy, spinal and brain trauma and other neuro-muscular disorders.

CHAPTER 3: Experimental Characterization of a Vector Doppler system

Vector Doppler systems use conventional pulsed wave Doppler from two or more independent directions using multiple transmitters or receiver pairs. This may be accomplished using multiple transducers arranged in a variety of geometric positions. The vector Doppler system estimates velocity vector from two or more independent directions. We accomplished this on a clinical scanner using the geometry seen in Fig.12.
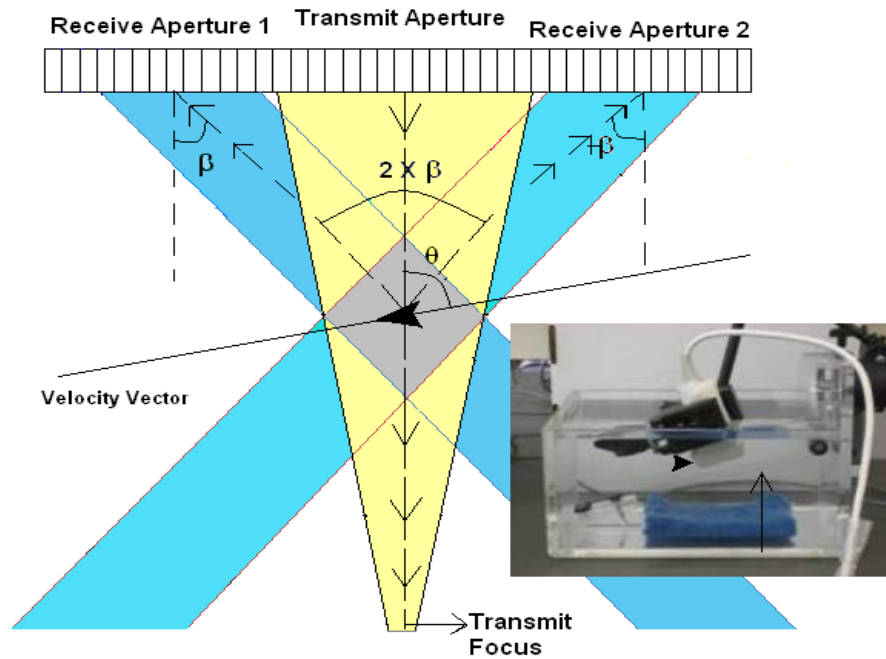
Figure12. Vector Doppler setup geometry. The yellow region represents the transmit aperture and the blue regions represent the receive apertures. Inset image shows the experimental setup. The arrowhead points to the transducer and the arrow points to the string driven by the motor.

Methods & Materials

The array transducer was divided into one transmit and two receive sub-apertures for these *in vitro* experiments. The transmit beam was normal to the ultrasound transducer. The receive apertures were steered at β, relative to the normal. This vector Doppler configuration was implemented on a Ultrasonix Sonix RP (Richmond, BC, Canada) ultrasound system with a 5-14 MHz linear array transducer probe, consisting of 128 elements and with a

38 mm field of view. The Sonix RP system has a research interface that enables low-level beamforming and pulse sequence control through a software development kit called Texo. This interface was used split the transducer into one transmit and two receive sub-apertures and steer the receive beams. The size of the beam overlap region was increased by de-focusing the transmit beam from the sample volume. The receive beams in this case are focused dynamically. The Doppler frequency was estimated from the both the receivers using the following equations:

$$v_1 = v\cos(\theta) + v\cos(\theta - \beta)$$
$$v_2 = v\cos(\theta) + v\cos(\theta + \beta) \tag{29}$$

Using Eq. 29 we get:

$$v = \sqrt{\left(\frac{v_1 + v_2}{2(1 - \cos\beta)}\right)^2 + \left(\frac{v_1 + v_2}{2\sin\beta}\right)^2} ; \theta = \tan^{-1}\left[\frac{1 + \cos\beta}{\sin\beta} \cdot \frac{v_1 - v_2}{v_1 + v_2}\right] \tag{30}$$

A calibrated Doppler string phantom (CIRS, Norflolk, VA, USA) was used for evaluating the accuracy of velocity vector estimation. The experimental setup consisted of a string (surgical 3-0) attached to a stepper motor driven pulley, as seen in Fig.12 (inset). The motor drive is programmable and can produce different waveforms. The transducer was positioned at different orientations using a clamp. The transducer and the clamp were immersed in an acrylic based water bath. The velocity of the string was controlled using an electronic controller connected to a stepper motor.

B-mode imaging was used to position the transducer probe over the string and measure the depth and orientation of the string relative to the transducer to an accuracy of 0.1mm and $\pm 2^0$ respectively. The pulse repetition frequency (PRF) was set to 10.44 KHz, the transmit frequency was 5MHz and size of the sub-apertures was 32 elements. The effect of the following four parameters on the velocity estimates was investigated:

 a. Receive beam steering angle (β)

 b. Depth of the string

 c. Angle of the velocity vector

 d. Depth of the transmit focus

The resultant velocity waveforms were compared to an ideal velocity waveform obtained using the string phantom specifications.

Signal Processing

The raw RF data was digitized at 40 MHz and analyzed offline using MATLAB (Mathworks, Inc., Natick, MA). The data were demodulated to base-band and filtered with a 100 Hz high pass filter to remove stationary and slow moving clutter. Mean velocities were estimated using conventional autocorrelation velocity estimator [19] with an ensemble size of 48. A correction term equal to one standard deviation was added to better estimate the Doppler spectral envelope. A median filter was employed to remove isolated velocity peaks. The noise was rejected below -6dB from the peak power signal.

Results

RF data were collected for a total of 33 *in vitro* tests over four scenarios. The velocity magnitude and direction were estimated. Fig.13 shows the vector Doppler displays for $\beta = 45$ and $\theta = 90$ & 75 respectively.
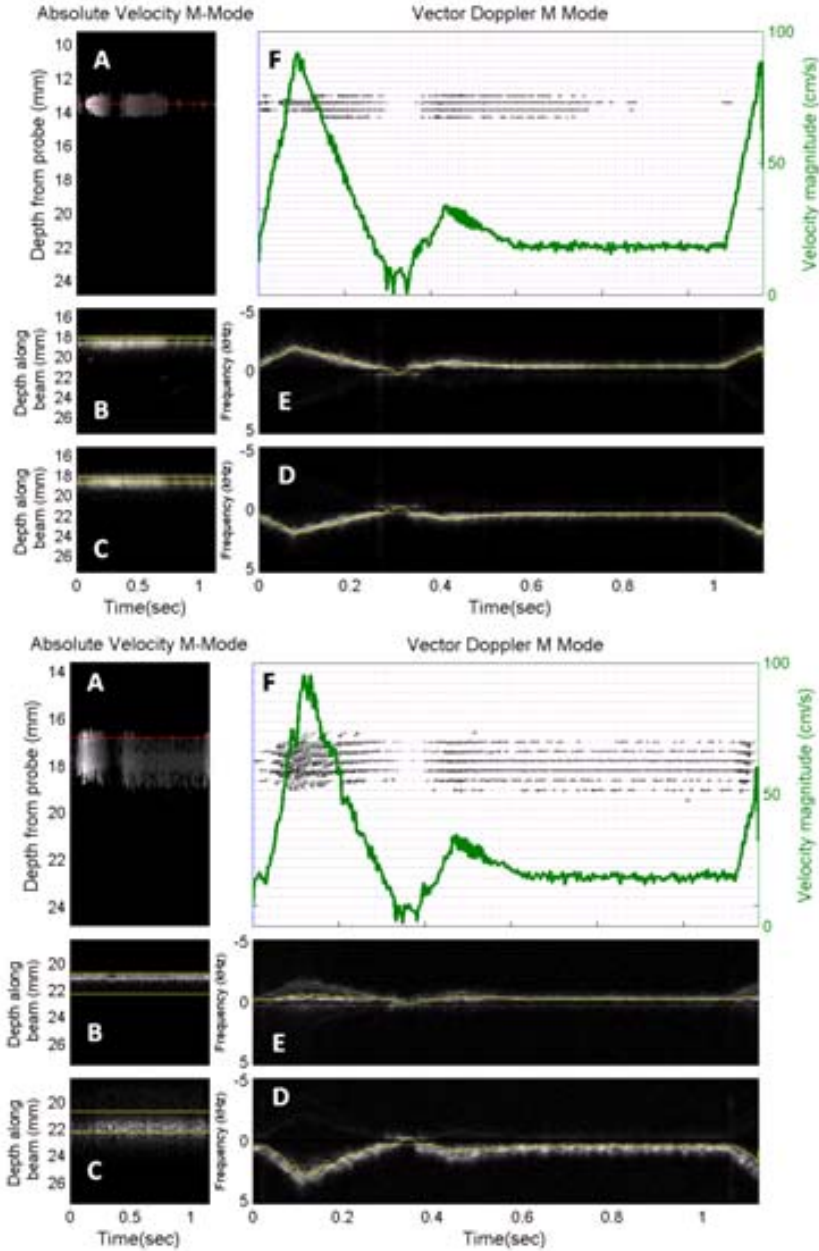
Figure13. Vector Doppler displays for $\beta = 45$ and $\theta = 90$ (top panel) and $\beta= 45$ and $\theta = 75$ (bottom panel). (a) The velocity magnitude displayed as an M-mode with depth from the transducer on the vertical axis and time on the horizontal axis. (b), (c) Echo M-mode with depth along the steered receive beam for receive apertures 1 and 2, respectively. (d), (e) The spectrogram of the received echoes from the region of interest for each receive apertures 1 and 2, respectively. (f) Velocity M-mode with arrows representing the flow vector.

Table1. Dependence of the estimated mean peak systolic velocity and angle estimates on the steering angle, focusing depth, depth and orientation of the string.

Scenarios	Steering angle, β (deg.)	Transmit focus depth (mm)	String angle, θ (deg.)	String depth (mm)	Mean abs. error in velocity (cm/s)	Standard deviation of error in velocity (cm/s)	Max abs error in velocity (cm/s)	Mean abs error in angle (deg.)	Standard deviation of error in angle (deg.)
1	15 (center of beam overlap: 22 mm)	12	90	23	9.64	9.94	43.76	2.84	1.26
2		23	90	23	7.00	9.29	39.20	2.75	1.15
3		40	90	23	8.30	9.40	42.21	2.17	2.15
4		60	90	16	4.74	3.97	20.28	0.72	1.03
5			90	18	5.39	2.99	16.02	0.55	0.42
6			90	20	7.40	4.07	23.51	0.67	0.49
7			90	22	9.22	4.56	26.28	0.73	0.88
8			75	16	8.48	5.23	25.34	4.64	1.9
9			75	18	6.39	3.83	23.61	3.78	1.99
10			75	20	6.73	4.13	18.80	4.16	2.57
11			75	22	5.33	4.15	27.36	3.1	2.12
12	30 (center of beam overlap: 21 mm)	12	90	23	7.14	4.79	23.36	1.56	1.05
13		23	90	23	8.08	5.50	29.60	1.23	0.88
14		40	90	23	3.09	3.15	16.77	1.77	0.88
15		60	90	16	2.16	2.56	13.12	0.93	1.14
16			90	18	3.70	2.85	20.90	0.68	0.59
17			90	20	3.53	2.36	12.93	0.99	1.3
18			90	22	5.69	5.07	29.40	0.82	0.56
19			75	16	8.67	4.91	25.09	1.85	1.23
20			75	18	6.52	4.11	26.11	5.37	2.59
21			75	20	6.06	4.27	21.81	3.37	2.18
22			75	22	5.04	5.11	26.41	4.76	2.41
23	45 (center of beam overlap: 12 mm)	12	90	18	5.58	3.26	19.71	2.44	3.52
24		18	90	18	7.71	5.45	26.90	0.84	0.97
25		30	90	18	4.38	3.92	16.35	1.89	0.67
26		60	90	12	2.56	2.53	11.95	0.23	0.24
27			90	14	3.52	3.67	19.75	0.4	0.39
28			90	16	5.85	4.08	22.27	0.51	0.48
29			90	18	9.37	6.28	31.04	0.56	0.75
30			75	12	3.66	4.03	20.95	5.06	3.49
31			75	14	2.80	2.27	10.80	4.39	2.2
32			75	16	2.95	3.00	16.63	8.33	2.46
33			75	18	4.66	4.85	30.01	6.13	1.22
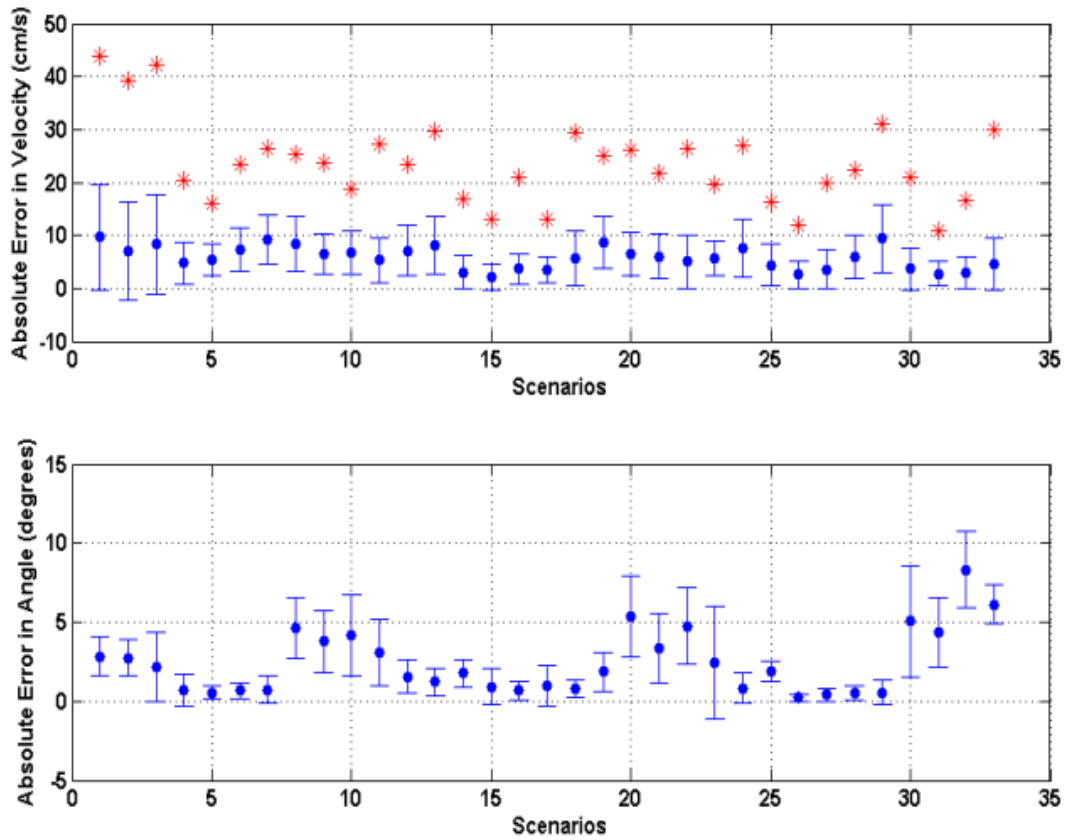
Figure14. Mean absolute error plots for velocity (top panel) and angle (bottom panel) estimates. The error bars represent standard deviations. The maximum absolute velocity error is indicated in red. The scenarios refer to column # 1 in Table 1.

Table1 and Fig.14 summarize the estimation errors for different experimental scenarios. The velocity and angle estimation errors were calculated using the ideal velocity waveform obtained from the string phantom specifications. The estimated velocity errors were comparable for all the test scenarios; however, the errors were largest for the 15^0 case. This is expected since the Doppler shifts are lower in this scenario. The maximum errors tend to occur at the velocity maxima or at the velocity minima.
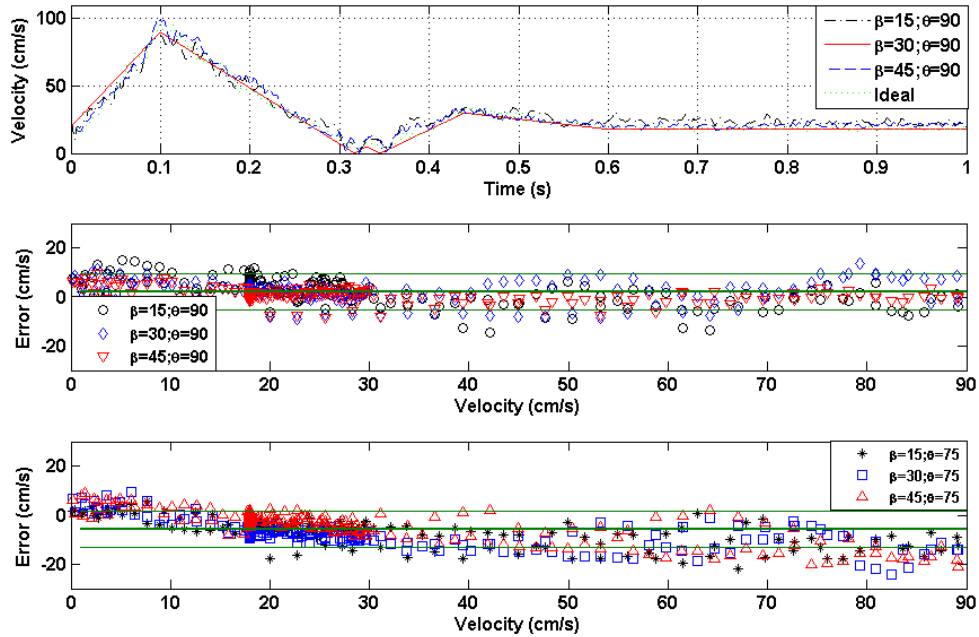
Figure15. Estimated velocity waveforms for three different steering angles compared to the ideal velocity waveform (top panel). Bland-Altman plots of velocity errors vs. velocity with different beam steering angles for $\theta = 90^0$ (middle panel) and $\theta = 75^0$ (bottom panel).

Fig.15 shows that the estimated velocity waveforms for different beam steering angles are similar to the ideal velocity waveform, and the estimation errors are similar although the velocity tends to be underestimate for the 75^0 beam to string angle.

We have demonstrated that a vector Doppler system can be easily implemented in a clinical setting for robust Doppler velocimetry. Our results showed that the four investigated parameters have a minimal effect on the velocity and angle estimates and can produce accurate measurements. The

next step is to investigate vector Doppler to measure musculoskeletal motion *in vivo*. We performed experiments on normal human subjects and in patients with cerebral palsy and foot drop and measured musculoskeletal motion using vector tissue Doppler imaging.

CHAPTER 4: Measurement of Rectus Femoris Muscle Velocities during Patellar Tendon Jerk using Vector Tissue Doppler Imaging

Introduction

Functional significance of muscle stretch reflexes is not entirely clear; however their role in sensation and control is evident [21]. Neurological abnormalities associated with stroke, brain and spinal cord trauma and many others cause abnormal change in reflex. The standard tendon tap test is a clinical measure of stretch reflex activity and excitability of the spinal cord. The tendon tap causes rapid lengthening of muscle, activating the Ia muscle spindle afferents and reflex monosynaptic activation of the spinal motoneuron pool of the muscle, resulting in the rapid knee extension.

Stimuli like the tendon tap are not encountered during normal movement activities. It is not known whether the muscle lengthening velocity during tendon tap approaches or exceeds those produced by the rapid stretch of limb segment, or how it compares to the range of knee angular velocities during normal functional activities. Previous studies have demonstrated that

50

in response to tendon tap, both rectus femoris and vastus lateralis muscles are activated through monosynaptic networks [22].

Ultrasound can easily and noninvasively visualize muscle motion. Tissue Doppler imaging can be routinely used in estimating skeletal muscle motion. Muscle motion is generally along the surface of the skin and conventional Doppler methods can only estimate muscle motion along the ultrasound beam, which is perpendicular to the muscle motion. Vector Doppler ultrasound can quantitatively access and measure the muscle elongation and activation velocities in two dimensions. We have developed a vector tissue Doppler imaging (vTDI) system by electronically splitting a linear array transducer into multiple sub-apertures that can be electronically be steered to estimate motion is multiple directions. These individual estimates can be used to obtain a velocity magnitude and direction in an angle independent manner.

The aim of this preliminary study was to use vTDI and evaluate the feasibility of:

1. Measuring *rectus femoris* longitudinal velocities during clinical tendon tap test.

2. Determining the transfer function between angular knee velocity and longitudinal *rectus femoris* velocity in healthy individuals.

3. Using the transfer function to calculate the knee angular velocity corresponding to tendon tap.

Methods & Materials

Six healthy volunteers (three men and three women, age 20-29 yrs) were recruited from the staff and students of George Mason University population and provided informed consent to participate in this study. Our institutional review board approved all procedures for this study.

The tendon of the knee quadriceps was tapped multiple times at different levels of manually controlled force. The impact of the hammer was recorded using an accelerometer (Omega Engineering. Inc., Stamford, CT). The knee angular motion was measured using an electrogoniometer (Biometrics Ltd., UK) attached to the knee joint. The *vastus lateralis* muscle instrumented with a surface electrode EMG (Motion lab System Ltd., Baton Rouge, LA).

The linear array transducer was divided into two transmit and two receive apertures and the beams were steered to an angle of 45^0. The velocity vector was reconstructed from individual velocity components described in detail by Dunmire et al. Velocity was estimated using conventional autocorrelation method and a correction equal to one standard deviation was applied.

Results

The rectus femoris muscle associated with the reflex response to a tendon tap has three peaks as shown in Fig. 16(E).
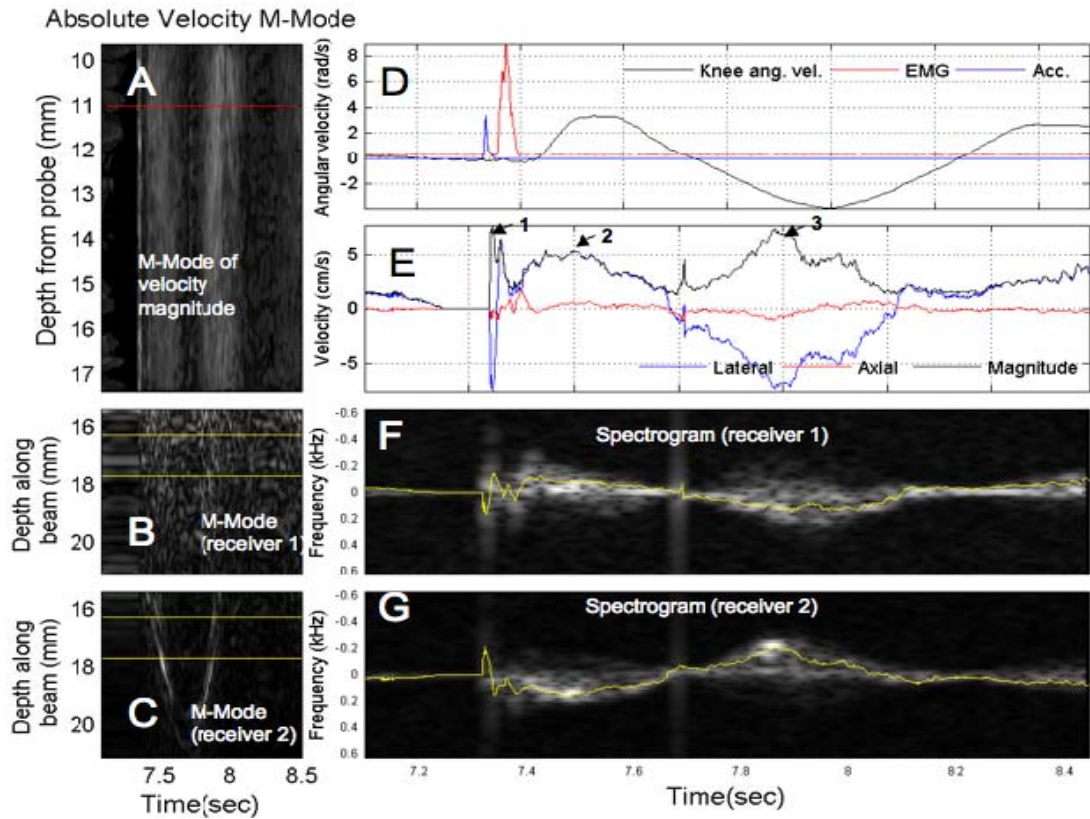
Figure 16. Vector Doppler display. (A) An M-mode display of the estimated velocity magnitude, with time on the horizontal axis and depth on the vertical axis. (B, C) M-mode of the received echoes by receivers 1 and 2, respectively. The yellow lines indicate the region of interest based on the center of the rectus femoris. (D) The joint angular velocity (black), EMG (red) and hammer acceleration signals (blue). (E) The estimated velocity magnitude and the axial (red) and lateral (blue) components. Arrows 1, 2, and 3 represent the elongation, reflex extension and passive flexion velocities. (F, G) Doppler spectrograms of echoes received by receivers 1 and 2, respectively. The yellow lines represent the detected velocities.

The first peak occurs immediately after the hammer impact and corresponds to elongation of the muscle due to tendon tap (v_{el}^{tap}). The second peak occurs after the EMG signal indicates the activation of the muscle due to a reflex extension (v_{sh}^{reflex}). The third peak is a passive flexion of knee

returning to its original position ($v_{el}^{passive}$). Muscle elongation velocity

$v_{el}^{passive}$ coincides with knee angular velocity $\omega_{el}^{passive}$. The transfer

function between ($\omega_{el}^{passive}$) and ($v_{el}^{passive}$). The equivalent knee angular

velocity (ω_{el}^{tap}) corresponding to the elongation of the *rectus femoris* muscle

during standard tendon tap can be estimated as follows:

$$\omega_{el}^{passive} = A \ X \ v_{el}^{passive} + B$$

(31)

$$=> \ \omega_{el}^{tap} = A \ X \ v_{el}^{tap} + B$$

Fig.16(A) shows M-mode display of the reconstructed velocity magnitude. The M-mode echoes received by the two receive apertures is shown in Fig.16(B) & (C) while their corresponding spectrograms are shown in (F) and (G). Table (2) summarizes the observed linear regressions between various measurements and estimated values for this study. The passive elongation velocity for the *rectus femoris* muscle measured using vector TDI correlated well with the angular velocity of the knee joint measured using

55

the electrogoniometer ($R^2 = 0.88$). Some cases had higher sensitivity to tendon tap than others, with a high correlation of $R^2 = 0.71$ and 0.96, for cases 4 and 5 respectively. Other cases had a lower correlation with the $R^2 = 0.03, 0.33, 0.25$ and 0.56 for cases 1, 2, 3 and 6 respectively.

Table2. Summary of all the observed linear regressions between various measurements and estimated values for this study.

Variables	R^2	Linear Regression
$\omega_{el}^{passive}$ and $v_{el}^{passive}$	0.88	$\omega_{el}^{passive} = 0.63 \text{ X } v_{el}^{passive} - 0.33$
$v_{el}^{passive}$ and $v_{ex}^{passive}$	0.80	$v_{el}^{passive} = 1.14 \text{ X } v_{ex}^{passive}$
EMG and v_{sh}^{reflex}	0.70	$\text{EMG} = 0.11 \text{ X } v_{sh}^{reflex} - 0.17$
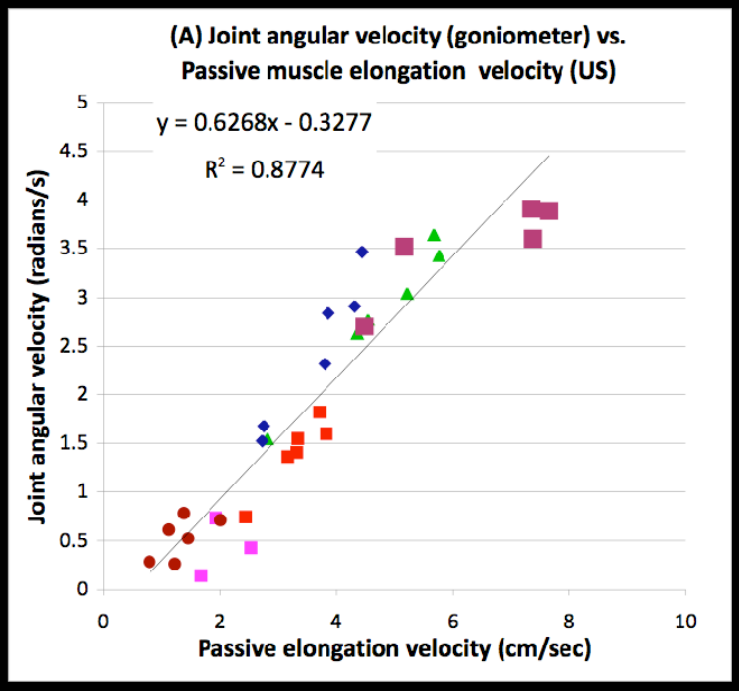
Figure17. The transfer function between the measured passive joint angular velocity using a goniometer, $\omega_{el}^{passive}$, and the passive muscle elongation velocity measured using US, $v_{el}^{passive}$.
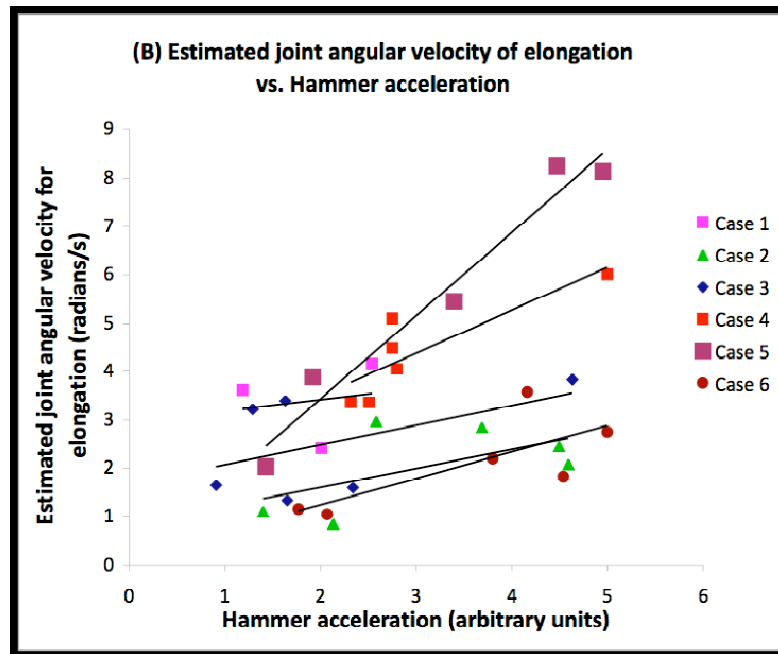
Figure18. The estimated joint angular velocity equivalent to the elongation produced by tendon tap, ω_{el}^{tap}, for different cases and different tapping strengths. Some cases had higher sensitivity to tendon tap, with a high correlation between ω_{el}^{tap} and the hammer acceleration (R2 =0.71 and 0.96, for cases 4 and 5 respectively), whereas other cases had lower sensitivity (R2 =0.03, 0.33, 0.25 and 0.56, for cases 1,2,3 and 6 respectively).

$$\alpha = 184.63 + 351.75 \ \omega \ ; \ r = 0.74$$

$$a = 111.16 + 351.76 \ v \ ; \ r = 0.74$$
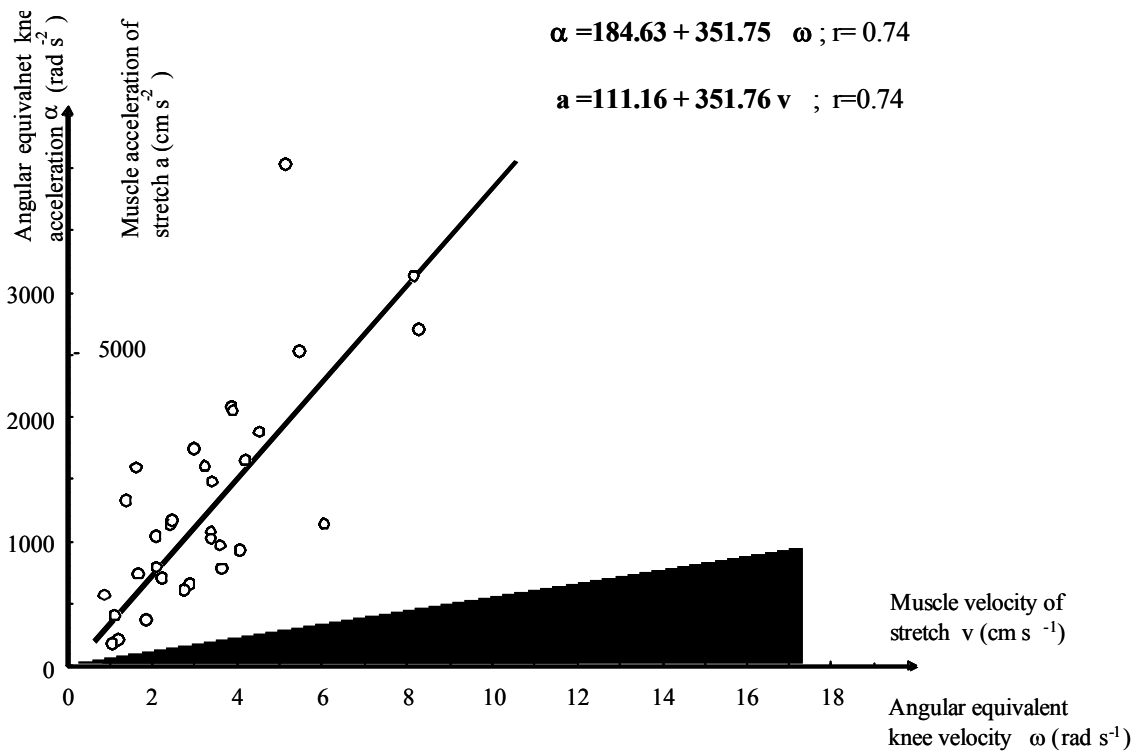
Figure19. The longitudinal kinematics (velocity v and acceleration a) of rectus femoris muscle and equivalent angular knee kinematics (ω and α respectively) during patellar tendon taps ranging from weak to strong. Note that knee angular equivalent acceleration but not velocity exceeds the ranges generated during voluntary knee flexion with maximum velocity, (shaded area) and during jump (dotted area,) as estimated from Lebiedowska, 2009 and Moran and Marshal, 2006 (respectively).

Our muscle lengthening velocity estimates obtained using vector tissue Doppler imaging during tendon tap agreed with velocity measurements made by Grubb et al. [32]. We think vector tissue Doppler imaging can be an effective method to measure the dynamics of musculoskeletal motion without the need to visualizing landmarks. Using this technique, we investigated the accuracy and repeatability of measuring *tibialis anterior* tendon velocities in patients with cerebral palsy and foot drop.

59

CHAPTER 5: Measurement of Tendon Velocities using Vector Tissue Doppler Imaging: A Feasibility Study

Introduction

Quantitative methods for direct measurement of muscle and tendon kinematics may lead to improved clinical outcome measures for neuromuscular and movement disorders, such as cerebral palsy (CP). Traditionally, joint kinematics, dynamometry and electromyography have been used as clinical outcome measures. In the recent years, ultrasound has become an important tool to directly measure the length, shape and deformation of skeletal muscles and tendons. Studies using ultrasound have been used to investigate functional changes in length and shape of muscle and tendons [24, 25]. Currently only a limited number of methods exist for estimating muscle and tendon motion using ultrasound. Most of these methods rely on landmarks in B-mode sequences such as a myotendenous junction. Some of the methods used to detect muscle and tendon motion include speckle tracking [3]; color Doppler [26] and elastography [27]. All these methods have limitations in quantitative accuracy of motion tracking.

Spectral Doppler has traditionally been a method of choice in cardiovascular applications. However, traditional 1D spectral Doppler has limitations in accurately estimating skeletal muscle and tendon motion since skeletal muscle motion is along the surface of the skin and normal to the ultrasound beam. To overcome this problem, we have come with a novel approach to estimate skeletal muscle and tendon motion in two dimensions using vector tissue Doppler imaging (vTDI).

Vector TDI estimates muscle and tendon motion in two dimension using two more transmit and receive pairs oriented in different directions. Vector Doppler combines velocity estimates from these independent transmit-receive pairs, producing a single angle independent velocity vector, with both magnitude and direction information [7, 8]. Since this method relies on spectral Doppler, it provides quantitative and accurate velocity estimates and has a higher temporal resolution over the other methods mention in detecting muscle and tendon motion. In preliminary studies, we have characterized the accuracy of this vector Doppler system [30] and also shown the feasibility of measuring muscle contraction velocities *in vivo* [31].

The vector TDI was developed on a clinical scanner with a research interface on a liner array transducer. This system has the ability to perform

experiments in a clinical setting simultaneous with a 3D motion capture system. Using vector Doppler, we evaluated the contraction velocities of *tibialis anterior* patients with cerebral palsy and foot drop. Foot drop is a condition where there is inadequate or loss of dorsiflexion due to a hypo-active or loss of activation of the common peroneal nerve. This causes a problem during the swing phase of gait making patients with this disorder to drag their foot as they walk. Measurements made using vector Doppler were compared with conventional joint kinematics estimated using an infrared 3D motion capture systems.

Methods & Materials

Vector TDI was implemented on a Ultrasonix Sonix Touch® ultrasound system with a 5-14 MHz linear array transducer with 60mm field of view. A SDK called Texo was used to split the linear array in two transmit and receive sub-apertures. The transmit and receive beams were steered by 15^0 with respect to the normal and the transmit beam focused at the center of the tendon. Transmit and receive apertures were set to 32 elements. The magnitude of the resultant velocity vector can then be obtained from the individual velocity components as described previously [6, 29]:

$$v = \frac{c}{4 f_t} \sqrt{(\frac{f_1 + f_2}{\cos\beta})^2 + (\frac{f_1 - f_2}{\sin\beta})^2}$$

(32)

where β is the beam steering angle, f_1 and f_2 are the two received frequency components and f_t is the transmit frequency.

This study was done at the Functional & Applied Biomechanics Section in the Rehabilitation Medicine Department of the National Institutes of Health, Clinical Center. Children with spastic cerebral palsy (CP) who could ambulate independently with no assistive device (Gross Motor Function Classification Scale level I & II) were evaluated. Those with a foot drop pattern identified by a physiatrist through clinical observation were eligible for the study. The exclusion criteria were administration of botulinum toxin to the *gastrocnemius* and *soleus* muscle groups within the past four months or during the study or surgery to the legs in the past year. The NICHD Institutional Review Board approved this study and all subjects and their caregivers provided informed consent and assent of a minor, respectively, to participate in this study.

All subjects were asked to sit comfortably in an upright position on a tall chair such that their feet did not touch the ground. To ensure good signal coupling, hypoallergenic transmission gel (Aquasonic 100, Parker laboratories, NJ) was applied on the skin surface at the ankle and a 2×9 cm stand-off pad (Aquasonic 100, Parker laboratories, NJ) was also used to avoid near field effects. The stand-off pad was held in place using polyvinylidene chloride (PVDC) wrap. A custom built US transducer holder made from gypsum plaster and a Neoprene cuff was used to stabilize the US transducer to the ankle (Fig.20) while allowing full ankle dorsiflexion. B-mode imaging was used to ensure that the center of the *tibialis anterior tendon* was located at the center of the expected beam overlap region. Subjects were asked to perform rapid ankle dorsiflexion and relaxation while data were being collected.

A Vicon 612 (Lake Forest, CA, USA) motion capture system was used to quantitatively measure ankle joint motion. A subject specific model was created using this motion capture system. Ten Infrared (IR) cameras were used to capture the motion of reflective markers placed at specific locations on the foot, ankle and lower leg (shank).
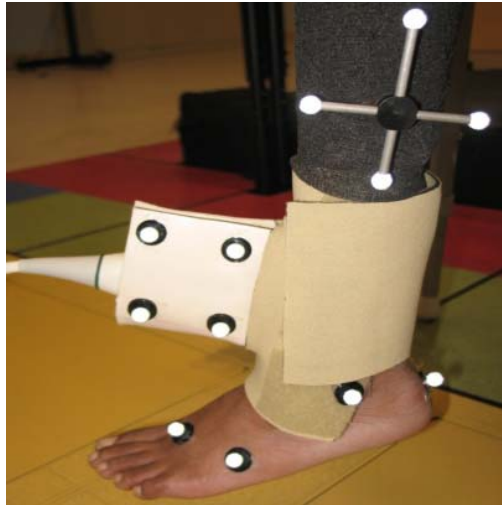
Figure20. The experimental setup for measuring *tibialis anterior* tendon velocities using ultrasound and IR motion capture system. The ultrasound probe was held in place using a custom holder and a Neoprene cuff, and reflective markers were placed on the probe and on anatomical landmarks.

Signal Processing

The ultrasound data acquired at 5-MHz transmit frequency were digitized at 40 MHz and processed offline using MATLAB (Mathworks, Inc., Natick, MA). A broadband velocity estimator based on the 2D Fourier transform was used for velocity estimation [20]. The raw RF signals from the two receive apertures were converted to analytical signals using the Hilbert transform. The signals from the two apertures were mixed to generate the sum and difference frequency components corresponding to axial and lateral components of the motion. The 2D Fourier transforms of these mixed signals were then computed to estimate variations of Doppler frequency with

RF. The Doppler spectra were estimated from projections of the 2D Fourier transform. The lateral velocity spectra, corresponding to the difference frequency, were obtained from a projection centered at zero frequency on the RF axis, while the axial velocity spectra, corresponding to the sum frequency, were obtained from a projection centered at twice the transmit frequency on the RF axis. Stationary and low-frequency clutter were removed using a 20-Hz high pass clutter filter. The mean and standard deviation of the Doppler spectrum were computed, and the envelope of the Doppler spectrum was estimated as the mean plus one standard deviation, with a correction for the variance of the analysis window. This envelope of the Doppler spectrum was used as the estimate of axial and lateral velocity components.

  Post processing of the raw data was done using Visual3D (C-Motion, Inc., MD). A bi-directional Butterworth low pass filter with a cut-off of 6Hz was used to remove any high frequency components produced due to vibration of the markers during motion of the ankle. The ankle angle time series waveforms were differentiated to obtain absolute joint angular velocity. The data were lowpass filtered at 5 Hz before calculating the velocity to remove transient noise.

Results

Absolute velocity waveforms were obtained from the TDI using Eq. (16).
Joint velocity waveforms were estimated from the displacement values of
the ankle obtained using the motion capture systems. Linear regression
analysis was used to compare the velocity values obtained using vector TDI
and the velocity values obtained using motion capture systems. The R^2 and
the error variance values of the regression line fit between the tendon
velocities obtained using vector TDI and the velocity values obtained using
motion capture system were computed for each trial.
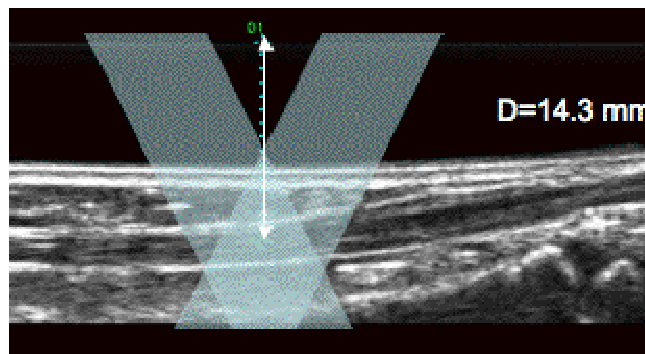
Figure21. B-mode image showing the *anterior tibialis* tendon visualized at a depth of
14.3 mm. The overlay denotes a schematic of the two ultrasound beams used for vector
Doppler imaging.

Fig.21 shows a B-mode image of the *tibialis anterior* tendon at a depth of
14.3 mm from the transducer. The overlay shows the expected ultrasound
transmit and receive beams from the two separate apertures interrogating the

tendon.

Fig.22 shows the correlations between the ultrasound and 3D motion capture measurements for one subject over multiple cycles of dorsiflexion and relaxation. Each cycle shows a distinct velocity peak corresponding to dorsiflexion and a higher velocity peak corresponding to the passive relaxation phase of the movement.
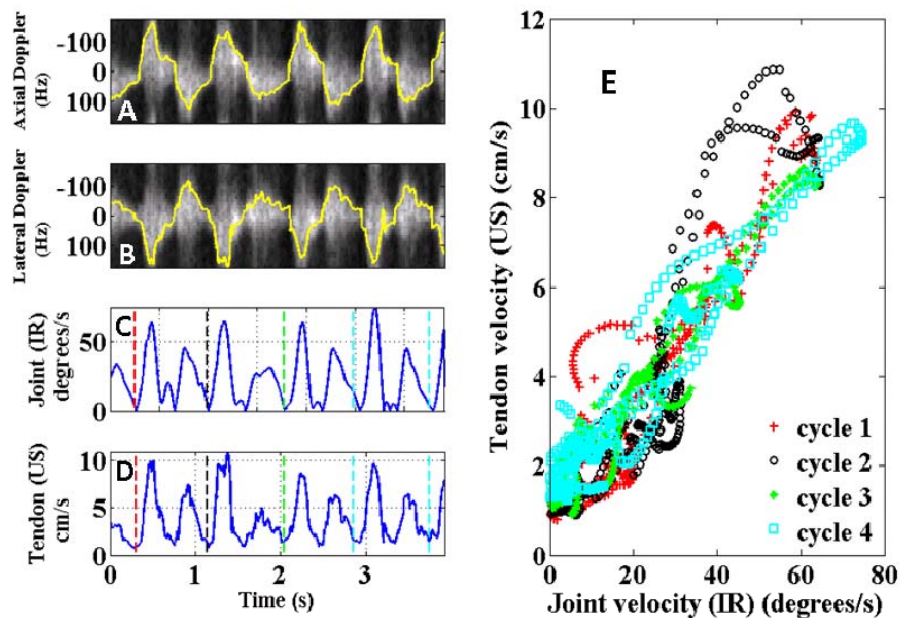
Figure22. Correlation between velocity waveforms measured using ultrasound and motion capture system. Four cycles of dorsiflexion and relaxation are shown. A & B display the axial and lateral spectrograms overlaid in yellow with the estimated velocities. (C) Joint velocity in degrees/s from motion capture system. D) Absolute tendon velocity using vector Doppler. (E) Correlation between velocity waveforms for all trials obtained from vector Doppler and motion capture systems.
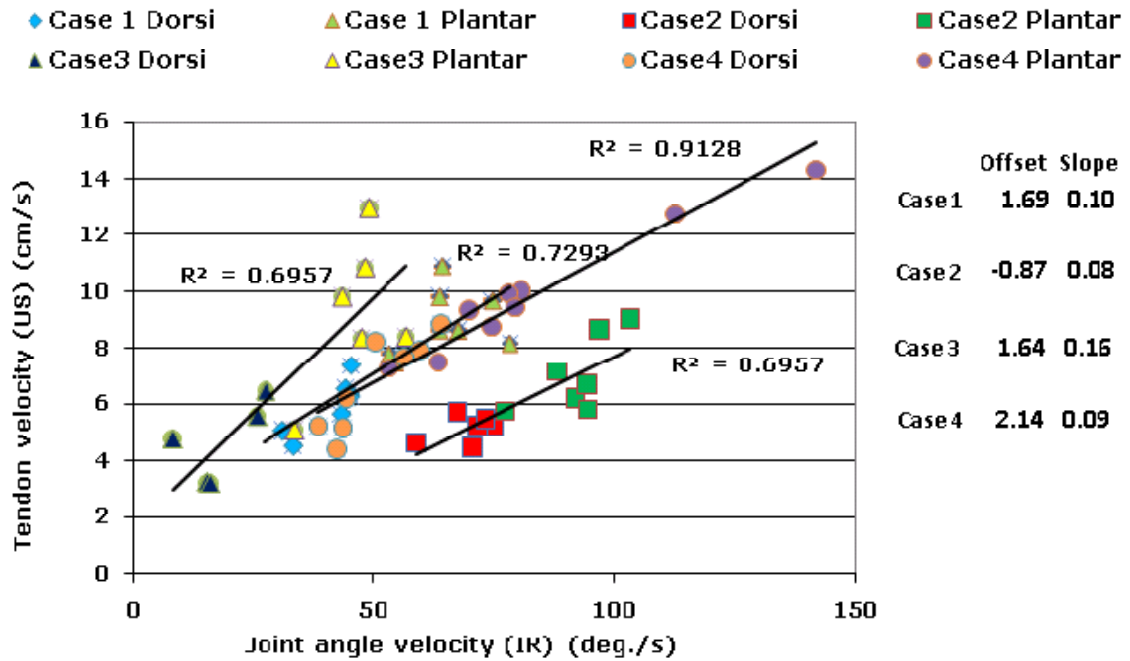
Figure23. Correlation between the peak velocities measured using ultrasound and 3D motion capture. For each subject, a linear relationship with strong correlation was observed between peak velocities for dorsiflexion and relaxation. Relaxation velocities were significantly higher than dorsiflexion velocities. Case 1 and Case 4 are the same subject studied 3 weeks apart.

Estimated absolute velocities from vector Doppler showed strong correlation with the estimated absolute velocities from the 3D motion capture system as shown in Fig.22 (E) and Fig.23. As expected, a linear relationship was observed between the joint velocity and the tendon velocity. Table 3 summarizes the R^2 values obtained over all the trials. The values over all trials are comparable with all 30 trials showing strong correlations, with peak velocity of 5.66±1.45 cm/s during dorsiflexion and peak velocity of

8.83±2.13 cm/s during passive relaxation.

Table 3. Summary of R^2 values between vector TDI and motion capture systems using linear regression.

Case	Trial	R^2	Case	Trial	R^2
1	1	0.77	3	1	0.64
	2	0.80		2	0.84
	3	0.77		3	0.78
	4	0.90		4	0.71
	5	0.84		5	0.80
	6	0.83		6	0.75
	7	0.94	4	1	0.88
	8	0.93		2	0.75
2	1	0.87		3	0.83
	2	0.79		4	0.85
	3	0.63		5	0.82
	4	0.76		6	0.85
	5	0.77		7	0.91
	6	0.75		8	0.71
	7	0.90		9	0.75

We have demonstrated that vector tissue Doppler imaging can be used to quantitatively measure tendon velocities. Our results show a strong correlation with data obtained from 3D motion capture system. Correlation results within the same patient showed repeatability. We are continuing to conduct clinical trial on patients with cerebral palsy and will compare with data collected from normal human volunteers.

CHAPTER 7: Discussion & Conclusion

***In Vitro* Experiments**

We developed a vector Doppler based on clinical ultrasound system with a linear array transducer for estimating velocity magnitude and direction. We characterized the accuracy of this system *in vitro* with the help of a calibrated string phantom. In particular we investigated the effect of change in four factors:

1. The beam steering angle
2. Angle of the velocity vector
3. Depth of the scatterer relative to the beam overlap region, and
4. The transmit focus depth.

Each of the above parameters was varied while keeping other three parameters constant as shown in Table 1. Our results indicate that the estimation errors are largely unaffected by the choice of the imaging system parameters. As expected, the maximum errors in velocity magnitude occurred for the 15^0 beam steering. Beam steering has been shown to cause errors in 1D pulsed Doppler [28], however we did not observe any major

differences in estimation error for 30^0 and 45^0 steering. The errors increased somewhat as the string was moved farther from the center of the beam overlap region. The mean errors were typically less than 10 cm/s (or 0.06×PRF), independent of the depth. These errors are similar to those reported in the literature [28].

The errors were sensitive to the method used for velocity estimation. The conventional autocorrelation method underestimated the velocities, especially during peak acceleration. After adding a variance correction term, the mean absolute estimation error decreased, while the maximum velocity errors increased for some scenarios. We believe that the maximum errors near velocity maxima were caused by increased variance due to spectral broadening, while those near the velocity minima were due to the suppression of low velocities by the clutter filter. More sophisticated velocity estimators can decrease the maximum errors. One approach is to use a wide band velocity estimator like the two dimensional Fourier transform. In this study, we did not investigate the impact of grating lobes due to beam steering. We intend to address the effect of grating lobes in future studies.

In this study, we utilized a single transmit aperture and two separate receive apertures. Other configurations are possible, such as two transmit and receive apertures [8, 29]. With our configuration, the path length of the ultrasound beam between transmit and receive is smaller than in the latter case, and the transmit path is shared between the receive apertures. We believe that this configuration would minimize any effects due to differences in the intervening tissues along the two paths.

A major advantage of using a linear array imaging transducer for performing vector Doppler is the ability to electronically control the receive beam steering, and aperture locations, for scanning a large field of view. Furthermore, duplex and triplex vector Doppler is possible, and conventional B-mode and color Doppler can be used to locate the region of interest for quantification of vector flow and tissue motion. Our results demonstrate that vector Doppler imaging using a linear array transducer is feasible for a wide range of imaging parameters and can be used for several *in vivo* investigations. The next set of experiments was conducted to measure the velocities of *rectus femoris* muscle on normal patients.

In Vivo Experiments: Mono-Synaptic Stretch Reflex

In this study, a novel vector TDI method was used to measure the rectus femoris muscle velocities during the monosynaptic stretch reflex response elicited by a patellar tendon tap. The direct measurement of the muscle velocity during elongation enabled us to estimate the joint angular velocity that is equivalent to the muscle stretch produced by the patellar tendon jerk. Our preliminary results indicate that the maximum joint angular velocity corresponding to tendon tap elongation is less than 8.5 radians/s, which is well within the normal range of angular velocities for the knee joint (upto 12 radians/s) [24].

Grubb *et. al.* measured the peak contraction velocities in the rectus femoris during a tendon tap test using the TDI M-mode available on conventional echocardiography systems. They measured peak contraction velocities of 5.6±1.3 cm/s to 8.1±1.6 cm/s in five subjects, which are comparable to the range of velocities measured in our study.

In our studies, the ultrasound transducer was externally clamped and the subject was seated on a fixed surface to minimize relative motion between the knee joint and the ultrasound probe due to the knee jerk. However, some relative motion was unavoidable. We believe that the impact of such relative

motion on our measurements was minimal, since we are measuring instantaneous muscle velocity. In the future, our methods can be extended to study more complex movements, as well as simultaneous measurement of the velocities of multiple muscle groups.

Other researchers have used ultrasound to measure fascicle stretch velocities during stretch reflex response [34, 35]. Typically, these methods involved the measurement and tracking of the fascicle length using B-mode ultrasound. This method has several limitations since the entire fascicle length for many muscle groups is difficult to measure due to the limited field of view of ultrasound and the measurements are sensitive to any movement of the transducer. The Doppler method overcomes these limitations since we are measuring the instantaneous velocity at a specified location without any need to visualize the entire fascicle.

We have successfully demonstrated that vector Doppler is capable of estimating longitudinal muscle velocities. While other researchers have developed custom vector Doppler instruments for blood flow imaging, a significant advantage of our approach is the use of a clinical ultrasound instrument, which would facilitate translation to clinical practice. We applied this vector tissue Doppler system to quantitatively measure the

velocity of the *tibialis anterior* tendon in patients with cerebral palsy and foot drop.

***In Vivo* Experiments: Quantitative velocity measurement of *tibialis anterior* tendon in patients with Cerebral Palsy and foot drop**

We investigated a vector TDI method to directly measure the velocity of *anterior tibialis* tendon during voluntary ankle dorsiflexion. As expected in patients with foot drop, we observed the peak tendon velocity during dorsiflexion was lower than during passive relaxation.

While the tendon velocities are expected to correlate with joint angle velocities, it is conceivable that in subjects with impaired movement, we would see differences between these two measures, which would indicate inefficiencies in movement control. Case 1 and case 4 were the same subject, but were studied 3 weeks apart. The slope of the trend line from linear regression analysis between tendon velocities and joint angle velocities in case 1 & case 4 were comparable, due the similar radius of motion of the subject. This shows that the velocity estimates obtained using vector Doppler are repeatable. We are continuing our studies in a population of subjects with foot drop before and after treatment using a device that

delivers surface electrical stimulation to the common peroneal nerve, triggered by tilt sensors on the lower leg, to initiate and maintain ankle dorsiflexion during the swing phase of gait for those with inadequate strength or control to accomplish this effectively.

The vector Doppler method overcomes several issues encountered with traditional spectral Doppler, which can only estimate motion only along the axis of the beam. The vTDI approach for estimating the tissue velocities could lead to better assessment of the magnitude and direction of tissue motion.

Some limitations of this study must be acknowledged. Although, Doppler methods are widely used in clinic for measuring velocities, various factors affect the accuracy of the measurements. The Doppler signal undergoes spectral broadening due the geometry of the vector Doppler system as well as during acceleration and deceleration. This increases the variance of the Doppler signal estimated using narrowband spectral estimators or autocorrelation-based estimators. We performed broadband estimation using the 2D Fourier transform to reduce the spectral variance. Additional signal processing strategies can further reduce the variance of the estimates. The location of the beam overlap region relative to the location of the tendon is

another consideration. In our experiments, we scanned through a large region of interest by electronically controlling the transmit and receive apertures. This enabled us to reconstruct anatomical images from each receiver to confirm the location of the tendon. The ability to perform simultaneous imaging is a significant advantage of performing vector Doppler using an array transducer. Another potential source of variation is the relative motion between the transducer and the shank during dorsiflexion and plantarflexion. In our experimental setup we used a custom holder and a neoprene cuff to stabilize the position of the transducer. In our future studies, we will track the motion of the transducer relative to the shank using the 3D motion capture system.

In summary, we have demonstrated that vector TDI is a feasible method for measuring tendon velocities *in vivo* using inexpensive equipment suitable for a clinical setting. We have also demonstrated that this technique can produce repeatable velocity estimates. Direct measurements of muscle and tendon velocities may be used as clinical outcome measures and for studying efficiency of movement control.

Appendix

Portions of Chapters 3, 4, and 5 were previously published in IEEE Conference Proceedings and are used with permission.

REFERENCES

REFERENCES

1. N. Pulkovski, P. Schenk, N. A.Maffiuletti and A. F.Mannion, "Tissue Doppler imaging for detecting onset of muscle activity," *J. Muscle & Nerve*, vol.37, pp.638-649, 2008.

2. C.N. Maganaris and J.P. Paul, "Tensile properties of the in vivo human gastrocnemius tendon," *J. Biomech.,* vol.12, pp. 1639-1646, 2002.

3. J.W.H. Korstanje et al., "Development and validation of ultrasound speckle tracking to quantify tendon displacement," *J. Biomech* (in press) 2010.

4. B.S. Cigali, et al., "Measurement of tendon excursion velocity with colour Doppler imaging: a preliminary study on flexor pollicis longus muscle," *European J. Radiology*, vol. 23, pp.217–221, 1996.

5. S. Ricci, S. Diciotti, L. Francalanci, and P. Tortoli, "Accuracy and reproducibility of a novel dual-beam vector Doppler method," *Ultrasound Med. Biol.*, vol.35, pp.829-838, 2008.

6. K.L. Hansen et al., "In vivo comparison of three ultrasound vector velocity techniques to MR phase contrast angiography," *Ultrasonics,* vol. 49, pp.659-667, 2009.

7. B. Dunmire and Kirk W. Beach, "Brief history of vector Doppler," *Proc. SPIE*, Vol. 4325, 200 (2001);

8. B. Dunmire, et al., "Cross beam vector Doppler ultrasound for angle-independent velocity measurements," *Ultrasound Med. Biol.*, vol.26, pp.1213-1235, 2000.

9. Satomura S.. Matsubara S. and Yoshioka M (1956) A new method of mechanical vibration measurement and its application. *Memoirs Inst. Scient. Indust. Res. Osaka Univ*. 13, 125-133.

10. J. Woo (2002, April). History of Doppler Ultrasound [Online] Available: http://www.ob-ultrasound.net/

11. D. W. Baker, "Pulsed Ultrasonic Blood Flow Sensing", *IEEE Trans Sonics Ultrasonics*, vol. 17, pp. 170, 1969

12. Fahrbach KK, "Apparatus for measuring the speed of flowing media," *US patent No. 3,* 1973; 766:517.

13. K.F. Bainton and M.G. Silk, "Some Factors Which Affect the Performance of Ultrasonic Transducers," *Br. J. Non-Destr. Test.* Vol. 22, no. 1, pp. 15-20. Jan. 1980.

14. J.W. Hunt, M Arditi, F.S. Foster, *"Ultrasound transducers for pulse-echo medical imaging," IEEE Trans Biomed Eng*. 1983 Aug;30(8):453-81.

15. G.S. Kino, C.S. DeSilets, "Design of slotted transducer arrays with matched backings," *Ultrason Imaging*. 1979 Jul;1(3):189-209.

16. N Aydin *and Evans*, "Quadrature-to-directional format conversion of Doppler signals using digital methods ," *Physiol. Meas.*, 1994 15 - 181.

17. J. A. Jensen, Stationary echo cancelling in velocity estimation by time-domain cross-correlation," *IEEE Trans. Med. Imag.*, vol. 12, no. , pp. 471-477, 1993.

18. Welch, PD; The Use of Fast Fourier Transform for the Estimation of Power Spectra: A Method Based on Time Averaging Over Short, Modified Periodograms", *IEEE Transactions on Audio Electroacoustics*, Volume AU-15 (June 1967), pages 70–73.

19. C. Kasai, K. Namekawa, A. Koyano and R. Omoto, "Real-time two-dimensional blood flow imaging using autocorrelation technique," *IEEE Trans. Sonics Ultrasonics*, vol. Su-32, pp.458-464, 1985.

20. T. Loupas and R.W. Gill, "Multifrequency Doppler: improving the quality of spectral estimation by making full use of the information present in the backscattered RF echoes," *IEEE Trans. Ultrasonics, Ferroelect. Freq. Contr.*, vol. 41, pp.522-531, 1994.

21. P. B. Matthews, "Restoring balance to the reflex actions of the muscle spindle: the secondary endings also matter," *J Physiol,* vol. 572, pp. 309-10, 2006.

22. J. D. Brooke, and W.E. McIlroy, "Movement modulation of a short latency reflex linking the lower leg and the knee extensor muscles in humans," *Electroencephalogr Clin Neurophysiol,* vol. 75, pp. 64-74, 1990.

23. K.A. Moran, B.M. Marshall, "Effect of fatigue on tibial impact accelerations and knee kinematics in drop jumps," *Med Sci Sports Exerc* 38:1836-42.

24. R.D. Herbert et al. "Change in length of relaxed muscle fascicles and tendons with knee and ankle movement in humans," *J. Physiol.*, vol. 539, pp. 637-645, 2000.

25. C.N. Maganaris, J.P. Paul, "Tensile properties of the in vivo human gastrocnemius tendon," *J of BioMech.,* vol. 12, pp. 1639-1646, 2002b.

26. J. Farron, T. Varghese, "Measurement of tendon strain during muscle twitch contractions using ultrasound elastography," *IEEE Trans. Ultrasonics, Ferroelectrics and Freq.Contro.,* pp. 27-35, 2009

27. B.S. Cigali, H.M. Buyruk, C.J. Snijders, J.S. Lameris, W.P.J. Holland, R. Mesut and H.J. Stam, "Measurement of tendon excursion velocity with colour Doppler imaging: a preliminary study on flexor pollicis longus muscle," *European J of Radiology*, vol. 23, pp. 217 – 221, 1996.

28. A. H. Steinman, A. C. H. Yu, K. W. Johnston and R. S.C. Cobbold, "Effects of beam steering in pulsed-wave ultrasound velocity estimation," *Ultrasound Med. Biol.,* vol. 31, pp. 1073-1082, 2005.

29. A. Pastorelli, G. Torricelli, M. Scabia, E. Biagi and L. Masotti, "A real-time 2-D vector Doppler system for clinical experimentation," *IEEE Trans. Med. Imag.,* vol. 27, pp.1515-1524, 2008.

30. A.Eranki and S. Sikdar, "Experimental characterization of a vector Doppler system based on a clinical ultrasound scanner," *Conf. Proc. IEEE EMBC,* pp. 2260-2263, 2009. [Used with permission (© 2009 IEEE).]

31. S. Sikdar, M. Lebiedowska, A. Eranki, L. Garmirian and D. Damiano, "Measurement of rectus femoris muscle velocities during patellar tendon jerk using vector tissue Doppler imaging," *Conf. Proc.IEEE in Med. & Biol.,* 2009, pp 2963-2966. [Used with permission (© 2009 IEEE).]

32. N. R. Grubb, A. Fleming, G. R. Sutherland *et al.*, "Skeletal muscle contraction in healthy volunteers: assessment with Doppler tissue imaging," *Radiology,* vol. 194, pp. 837-42, 1995.

33. M. E. Houston, R. W. Norman, and E. A. Froese, "Mechanical measures during maximal velocity knee extension exercise and their relation to fibre composition of the human vastus lateralis muscle," *Eur J Appl Physiol Occup Physiol,* vol. 58, pp. 1-7, 1988.

34. N. J. Cronin, J. Peltonen, M. Ishikawa *et al.*, "Effects of contraction intensity on muscle fascicle and stretch reflex behavior in the human triceps surae," *J Appl Physiol,* vol. 105, pp. 226-32, 2008.

35. K. Nakazawa, S. I. Yamamoto, T. Ohtsuki *et al.*, "Neural control: novel evaluation of stretch reflex sensitivity," *Acta Physiol Scand,* vol. 172, pp. 257-68, 2001.

36. R.E Zierler, et al. "Noninvasive assessment of normal carotid bifurcation heamodynamics with color-flow ultrasound imaging," *Ultrasound Med. Biol.,* vol. 13, pp. 471-479, 1987.

CURRICULUM VITAE

Avinash Eranki joined George Mason University in 2007 to pursue his Master of Science in Electrical Engineering. He was admitted to the PhD in Electrical Engineering in 2010. He received his Bachelor of Engineering from Visveswariah Technological University, India in 2007. He has been actively working with the Rehabilitation Medicine department at the National Institutes of Health since 2009. He has also worked at Aerospace Electronics and Systems Division at the National Aerospace Laboratories, India in 2007 on a novel signal processing approach to de-noise speech signals using filter banks. His interests involve novel applications of ultrasound imaging. He is working on developing new Doppler ultrasound and signal processing approaches for detecting and quantifying dynamics of musculoskeletal motion.